Univerzita Karlova v Praze

Matematicko - fyzikální fakulta

DIPLOMOVÁ PRÁCE

Aleš Růžička

Studium transportních vlastností některých polymerních vrstev

Katedra makromolekulární fyziky

Vedoucí diplomové práce: doc. RNDr. Jana Toušková, CSc.

Studijní program: Fyzika

Studijní obor: Fyzika kondenzovaných soustav a materiálů

Praha 2013

Charles University in Prague

Faculty of Mathematics and Physics

MASTER THESIS

Aleš Růžička

Study of transport properties of some polymer layers

Department of Macromolecular Physics

Supervisor of the master thesis: doc. RNDr. Jana Toušková, CSc.

Study programme: Physics

Specialization: Physics of Condensed Matter

Prague 2013

First of all, I am very thankfull to my supervisor doc. RNDr. Jana Toušková, CSc. for her guidance through both experimental and theoretical part of the diploma thesis and for an enormous amount of time which she invested in many fruitfull discussions with me.

Then I would like to thank the help of doc. RNDr. Jiří Toušek, CSc. especially during the experimental work and during preparation of the samples.

I am indebted to doc. Ing. et Ing. Ivo Kuřitka, Ph.D. et Ph.D. and to Ing. Pavel Urbánek for the preparation of the samples at Tomas Bata University in Zlin.

I am thankfull to RNDr. Věra Cimrová, CSc. for the evaporation of the samples and for her help and motivation during the final part of the work.

Many thanks go to kind scientists who made various measurements for my thesis, especially to doc. RNDr. Josef Pešička, CSc. for the transmission electron microscopy measurements and to Mgr. Jaroslav Kousal, Ph.D. for the ellipsometry measurements.

I am gratefull to Milan Růžička for the language corrections.

The last but not least I am very thankfull to my family and to my friends because I could not complete this thesis without their help.

I declare that I carried out this master thesis independently, and only with the cited sources, literature and other professional sources.

I understand that my work relates to the rights and obligations under the Act No. 121/2000 Coll., the Copyright Act, as amended, in particular the fact that the Charles University in Prague has the right to conclude a license agreement on the use of this work as a school work pursuant to Section 60 paragraph 1 of the Copyright Act.

In ..... date ..... Aleš Růžička

Název práce: Studium transportních vlastností některých polymerních vrstev

Autor: Aleš Růžička

Katedra / Ústav: Katedra makromolekulární fyziky

Vedoucí diplomové práce: doc. RNDr. Jana Toušková, CSc., Katedra makromolekulární fyziky

Abstrakt:
Tato práce zkoumá různé vlastnosti polymerních vrstev a hybridních vrstev obsahujících anorganické nanočástice. Vrstvy z MEH-PPV a polythiofénu jsou charakterizovány pomocí různých experimentálních technik. Temnostní voltampérové charakteristiky byly měřeny při různých teplotách a pohyblivost děr byla určena pro několik případů. Spektra fotonapětí jsou použita k vyhodnocení difúzní délky excitonů a SPV metoda je popsána. Dále je zkoumán vliv anorganických nanočástic CdS a ZnO na polymerní vrstvy pomocí různých experimentálních metod a jsou popsány možné aplikace těchto vrstev v hybridních solárních článcích. Distribuce velikostí anorganických nanočástic byly získány pomocí několika experimentálních přístupů, přičemž obdržené výsledky souhlasí s předpoklady.

Klíčová slova: polymerní vrstvy, transport náboje, hybridní solární články, anorganické nanočástice

Title: Study of transport properties of some polymer layers

Author: Aleš Růžička

Department: Department of Macromolecular Physics

Supervisor: doc. RNDr. Jana Toušková, CSc., Department of Macromolecular Physics

Abstract:
This work studies various properties of polymer layers and hybrid layers containing inorganic nanoparticles. MEH-PPV and Polythiophene films are characterized by different experimental techniques. Dark J-V characteristics were measured at different temperatures and the mobility of holes was evaluated in a few cases. Photovoltage spectra are used for a determination of the exciton diffusion length and the SPV method is discussed. The influence of the inorganic nanoparticles CdS and ZnO incorporated into the polymer layers is studied by various experimental methods and the applications of these layers in the inorganic-organic hybrid solar cells are discussed. The inorganic nanoparticle size distributions are obtained by several experimental techniques and the results correspond with the assumptions.

Keywords: polymer layers, charge transport, hybrid solar cells, inorganic nanoparticles

Contents

Preface

Scientists and researchers all over the world try to develop new and better electronic devices. A very interesting field which will be discussed in this diploma thesis is definitely the branch of conducting polymer materials. In the last few decades polymers have been a field of science which is able to attract enormous attention. Important milestone of polymer science was the year 2000 when A.J. Heeger, A.G. MacDiarmid and H. Shirakawa were awarded by the Nobel Prize for Chemistry.

Conjugated polymers (polymers where every second bond is a double bond) are very promising materials in several applications. Presented thesis will mainly describe different properties of conjugated polymers which are important for operation of organic solar cells. But conjugated polymers have a lot of other applications - for example, OLED (Organic Light-Emitting Diode) devices are very promising and they are fabricated for different purposes. OFET (Organic Field-Effect Transistor) or different optical memories are other promising applications of conjugated polymers. Organic materials in general are cheap and it is possible to produce different devices using wide range of preparation techniques.

Another interesting way to produce efficient organic solar cells, is combining both organic and inorganic materials together with improving properties of both parts. This quite new approach can combine advantages of well-known inorganic materials together with cheap and easily prepared organic materials.

This diploma thesis is divided into several parts. In Part 1, theory of different electrical and optical properties of polymers is given, together with some basic information about interesting properties of inorganic nanoparticles. Part 2 presents preparation of various samples which were measured and Part 3 is focused on different experimental techniques which were used during measurements of the experimental data for this diploma thesis. Part 4 describes all obtained experimental data and one can find discussions about the measured data in this part. Evaluation of different parameters is also present in Part 4. In the last part - Part 5 of the thesis, there is the conclusion containing the most important results of this work.

Part I

Theoretical background

This chapter is divided into three parts which characterize different types of the charge transport in polymer layers (and polymer films with nanoparticles), having regard to the use in organic semiconducting devices, especially in the organic solar cells.

1 Electrical conduction in polymers

Electrical conduction may occur through the movement of either electrons, holes or ions. Basic equation for conductivity σ is

$$\sigma = qn\mu \tag{1.1}$$

where q is the charge, n is the concentration of the carriers and μ is the mobility of the carriers. Values of the mobility μ and the conductivity σ for different materials are shown in Fig.1.1.

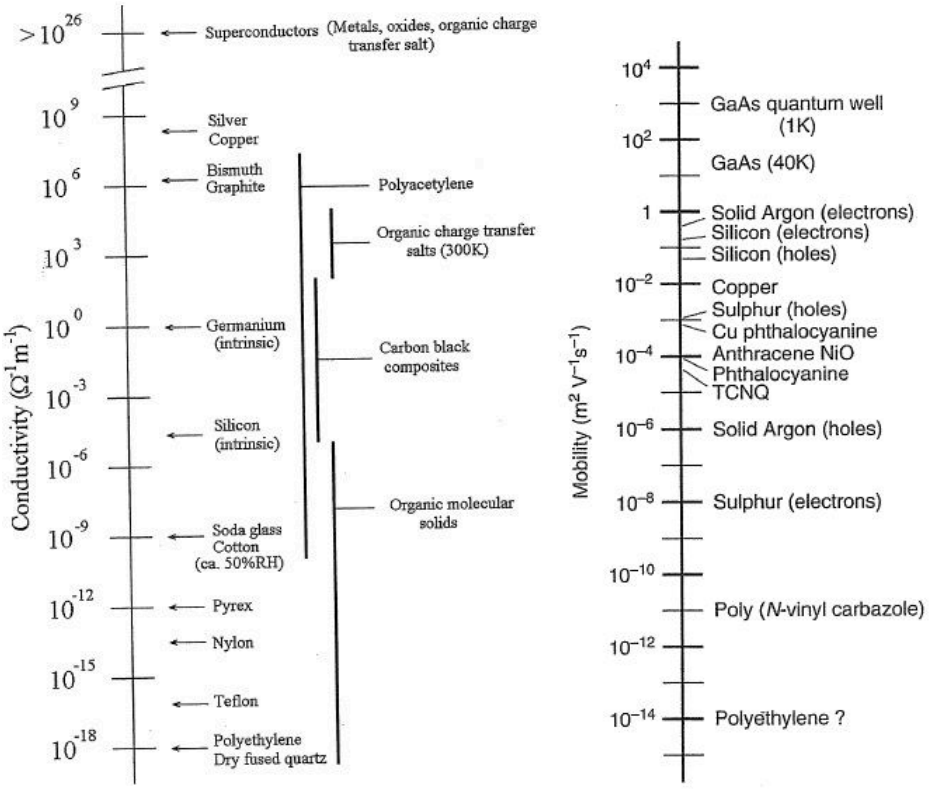

Figure 1.1: Chart of typical conductivities (left) and typical mobilities (right) [4]

There are generally two different types of dark transport (charge transport where illumi-

nation does not take part) present in organic semiconducting materials. These two types are "bulk-limited" and "injection (or contact)-limited" transport.

1.1 Injection-limited transport

The interface between the polymer material and the contacting electrode generally plays an important role in operation of different organic electronic devices. If the bottleneck in charge transport is the injection at the contacts, an electronic device operation is injection or contact-limited. The band offset between the metal work function and the LUMO (Lowest Unoccupied Molecular Orbital) or HOMO (Highest Occupied Molecular Orbital) level is an important factor in determining the type of contact at the interface (see Fig. 1.2).

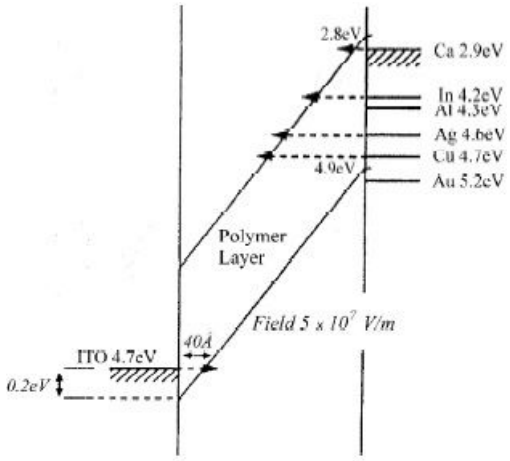

Figure 1.2: Materials which are usually used as contacts with their work functions

In the case of sizable potential energy barrier from metal into the transporting band, the charge injection would be poor and the contact resistance will dominate the device operation. Very common theoretical model which is used to explain the charge injection is the thermionic emission model.

Upon acquiring enough thermal energy, a carrier overcomes the intrinsic potential barrier Δ at the interface and the carrier is then injected into the polymer: $\Delta = W - I_p$, where W is the metal work function and I_p is the ionization potential of the organic material (see Fig. 1.3).

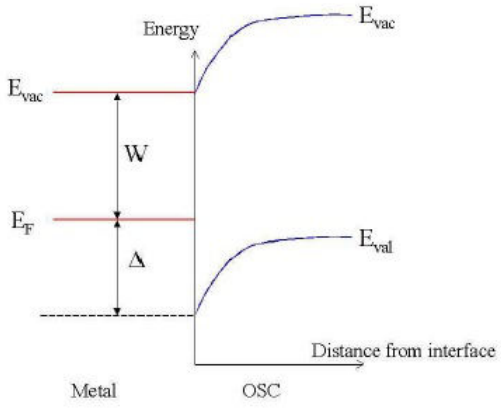

Figure 1.3: Scheme of the thermionic emission model [15]

The effect of Δ is modified by contributions from the external electric field potential and the image charge potential. Therefore, we obtain following equation ([43]) :

$$J = \frac{qm^*}{2\pi^2\hbar^3}(k_BT)^2 \exp(-\frac{q\Delta}{k_BT}) \exp(o)^{1/2}[\exp(\frac{qV}{k_BT}) - 1] \tag{1.2}$$

where q is the elementary charge,$m^*$is the effective mass, $\hbar$ is the reduced Planck´s constant, T is temperature, k_B is Boltzmann constant, J is the current density and V is the voltage.

The second exponential part in Eq. 1.2 accounts for the lowering of the barrier height due to the electric field at the interface and $o = q^3F/4\pi\epsilon_0\epsilon_r k_B^2T^2$, where F is the field, ϵ_0 is the permittivity of the vacuum and ϵ_r is the relative permittivity.

Thermionic emission is usually more significant at high temperatures where the carriers have sufficient thermal energy to overcome the potential barrier. At very low temperatures or in the cases where the height of the potential barrier is relatively large, thermionic emission usually loses its significance. On these occasions, charge carriers are injected only by means of quantum mechanical tunneling through the barrier. This process is called field emission and is the dominant injection-limited mechanism at high fields and low temperatures. Process of tunneling will be discussed later. [15]

1.2 Role of traps in organic materials

This part is mainly cited from Ref. [8].

Capture of the carriers in localized states involved in electrical transport may occur in two cases. Trapped carriers can be released after a specific period or they can recombine with carriers of opposite charge sign. If the release rate is higher than the recombination rate, the localized state is called a trap and for a dominant recombination, the localized state is a recombination centre. These two kinds of localized states can change from one to another because of conditions such as temperature and the ratio of the minority to majority

carrier concentration. Generally, both localized states mentioned above are sometimes called "trap", although their action is different.

Trapped charge carriers do not take part in the charge transport, the traps however affect the conduction in the material. Although the carriers are trapped, their columbic force influences the electric field distribution and the transport itself. Talking about inorganic semiconductors, we can say that the trap states are located in the energy gap. We can distinguish between an electron trap (it is able to trap electron) and a hole trap which is able to trap a hole.

The situation in organic semiconductors is more complicated. The density of states (DOS) in amorphous organic thin films is usually represented by a Gaussian-like distribution of localized molecular orbitals. The charge transport in such amorphous layer is mainly determined by hopping processes among strongly localized molecular states. The problem could be how to distinguish between a trap state and a regular transport state.

One possibility of solving this problem is by the transport energy concept. A carrier in a deep tail state will most probably escape to a state of energy E_t independent on its initial energy in the tail. E_t is called "transport energy" (escape energy) and it shows the level from which a trapped carrier is most probably released to move to a neighbouring site. Each state below E_t is a trap state and states above the transport energy are transport states, despite the fact that all states are localized. The transport energy is also a function of temperature, so, for instance, a state acting as a trap state at higher temperature may become a transport state at lower temperatures. There may exist additional trap states at a discrete energy level or with any energy distribution in the gap below transport energy. Concept proposed in this paragraph is shown in Fig.1.4. [33]

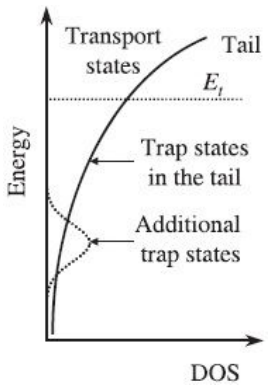

Figure 1.4: Trap states in the tail [8]

Some possible sources for trap states are :

impurities - A trap state is formed when the LUMO or HOMO of an incorporated molecule is situated in the gap of the host molecules.

geminate pairs - Coulomb interaction is usually strong in polymers, so both the hole and the electron can be affected by this interaction even if they are separated by several

molecules. A geminate pair is a pair of Coulomb bond charge carriers. If the recombination probability between the hole and the electron is suppressed by selection rules, a geminate pair forms a Coulomb trap.

structural defects - The LUMO/HOMO levels may vary from molecule to molecule. The exact energy position of the LUMO/HOMO could be determined not only by the chemical structure of the molecule but also by the polarisation of the surroundings or by the effective conjugation length in polymers.

self-trapping - This kind of trap state is connected with the effects of (bi)polarons. Polarons and bipolarons are mobile and thus are not traps in the original sense of the word. Their mobility is, however, lower than the mobility of free carriers. In polythiophene or polyacetylene the (bi)polaron formation causes significant lowering in energy. In this case, the charge carrier forms its own trap state on the polymer chain.

The next section is taken from Ref. [21, 11, 23].

All semiconducting organic materials have a large density of hole and electron traps. When the trap depth is large or the temperature is very low (it means that the trap levels are below the Fermi level), majority of the injected carriers is trapped. Both the trapped and the free charge carriers determine the space charge and the current is space charge limited (SCLC).

The Poisson equation is

$$\frac{dF(x)}{dx} = \frac{q}{\epsilon_r \epsilon_0}(p(x) + p_t(x)) \tag{1.3}$$

where F is the electric field, p is the free hole density, p_t is the trapped hole density.

In the following part, we assume that the traps are uniformly distributed in space but they might have a different distribution in the energy space.
Four different distributions in the energy space are considered :

(1) all traps at a single energy level

(2) a Gaussian distribution of traps in the energy space

(3) exponentially distributed traps in the energy space

(4) uniformly distributed traps in the energy space

1.3 Single level traps

Distribution of the traps for single energy level is

$$h(E) = H_d \delta(E - E_t) \tag{1.4}$$

where H_d is the trap density, δ is the Dirac delta function and E_t is the trap depth. The solution of the transport and Poisson equations gives

$$J = \frac{9}{8}\theta_a \epsilon_r \epsilon_0 \mu \frac{V^2}{h^3} \tag{1.5}$$

where h is the total thickness of the sample.
θ_a is given as

$$\theta_a \equiv \frac{p}{p + p_t} \tag{1.6}$$

If there are no traps in the material, density of traps p_t is zero and then $\theta_a = 1$. For these circumstances, Eq.1.5 changes to Child´s law for space charge limited currents (SCLC) :

$$J = \frac{9}{8}\epsilon_r\epsilon_0\mu\frac{V^2}{h^3} \tag{1.7}$$

Usually $p_t \gg p$ unless the applied voltage is very high. Then θ_a is the ratio of free to trapped carriers.

When the applied voltage is very low, the injected effective carrier density may be lower than the background thermal carrier density. In this case, the current is ohmic. SCLC begin to dominate at voltage V_Ω, which is given by relation

$$V_\Omega = \frac{8}{9}\frac{qp_0h^2}{\theta_a\epsilon_r\epsilon_0} \tag{1.8}$$

1.4 Gaussianly distributed traps

Distribution of traps in the energy space is given by

$$h(E) = \frac{H_d}{(2\pi)^{1/2}\sigma_t}\exp[-\frac{(E - E_{tm})^2}{2\sigma_t^2}] \tag{1.9}$$

where E_{tm} is the trapping energy at the maximum trap density and σ_t is the standard deviation of the Gaussian distribution.
If the relation $E_{tm} < E_{F_p}$ (shallow traps) is valid, then the ratio θ_d of free to trapped holes is given by

$$\theta_d = \frac{p(x)}{p_t(x)} = \frac{N_v}{H_d}\exp[-\frac{E_{tm}}{kT} + \frac{1}{2}(\frac{\sigma_t}{kT})^2] \tag{1.10}$$

Then the current density $J(V)$ is given as

$$J = \frac{9}{8}\mu\epsilon_0\epsilon_r\theta_d\frac{V^2}{h^3} \tag{1.11}$$

In the case when the trap depth is larger than the Fermi energy level ($E_{tm} > E_{F_p}$, deep traps), the $J - V$ relation is

$$J = \frac{N_V\mu_p}{q^{m-1}}(\frac{2m+1}{m+1})^{m+1}(\frac{m}{m+1}\frac{\epsilon\epsilon_0}{H_d'})^m\frac{V^{m+1}}{h^{2m+1}} \tag{1.12}$$

where

$$H_d' = \frac{1}{2}H_d\exp(\frac{E_{tm}}{mk_BT}) \tag{1.13}$$

and m is given by relation

$$m = (1 + \frac{2\pi\sigma_t^2}{16k_B^2T^2})^{1/2} \tag{1.14}$$

The expression for V_Ω for deep Gaussian traps is given by

$$V_\Omega = \frac{qd^2H_d'}{\epsilon_r\epsilon_0}\frac{m+1}{m}(\frac{m+1}{2m+1})^{\frac{m+1}{m}}(\frac{p_0}{N_V})^{\frac{1}{m}}$$

1.5 Exponential Traps

The concentration of the traps distributed exponentially in energy is

$$h(E) = \frac{H_b}{k_BT_c}\exp(-\frac{E}{k_BT}) \tag{1.15}$$

where H_b is the density of traps and T_c is the characteristic distribution constant. Trapped hole density is given by

$$p_t = \alpha H_b(\frac{p}{N_V})^{\frac{1}{l}} \tag{1.16}$$

where $l = \frac{T_c}{T}$. The factor $\alpha = (\pi/l)(\sin(\pi/l))$ is usually taken as unity.

Finally, following analytical expression for $J(V)$ can be obtained :

$$J = \frac{\mu_pN_v}{q^{l-1}}(\frac{2l+1}{l+1})^{l+1}(\frac{l}{l+1}\frac{\epsilon_r\epsilon_0}{\alpha H_b})^l\frac{V^{l+1}}{h^{2l+1}} \tag{1.17}$$

The Eq.1.17 is similar to Eq.1.12 but parameters l and m are different.

Example of typical $J-V$ characteristics of several organic materials are shown in Fig. 1.5.

There are three regions A, B, C and two transition regions T_1 and T_2. Region A and the transition region T_1 arise due to background doping or due to thermal carriers ([19]). Line B is the region of the space charge limited current which is controlled by the exponentially distributed traps. At higher voltages, the current deviates from the straight line B and the $J-V$ curve bends down and it changes to the transition region T_2. [20]

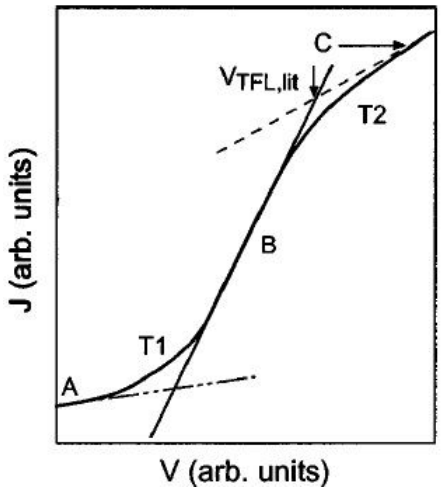

Figure 1.5: Scheme picture of typical J-V characteristics behavior for SCLC model [20]

1.6 Effect of Non-Zero Schottky Barrier

The theory of transport in insulators (including organic polymers) assumes that barrier for injection from metal (contact) into the organic layer is zero, so the contact is ohmic. But for most anode/cathode materials, the Schottky barrier ϕ_B is not zero.

Assuming exponential trap distribution and combining continuity and Poisson equations and after integrating the result equation, one should obtain

$$F(x) = (\frac{qH_b}{\epsilon_r\epsilon_0}\frac{(l+1)}{l}(x+C))^{\frac{l}{l+1}}(\frac{J}{q\mu N_V})^{\frac{l}{l+1}} \tag{1.18}$$

where C is the constant of integration.

Taking $\alpha = 1$ and after using boundary condition $V = \int_0^d F(x)dx$, we get

$$J = \frac{\mu_p N_v}{q^{l-1}}(\frac{2l+1}{l+1})^{l+1}(\frac{l}{l+1}\frac{\epsilon_r\epsilon_0}{H_b})^l \frac{V^{l+1}}{[(h+C)^{\frac{2l+1}{l+1}} - C^{\frac{2l+1}{l+1}}]^{l+1}} \tag{1.19}$$

For applied voltage V or given current J, the constant of integration C is independent of $F(x)$ and x. At the injecting contact, we assume $x = 0$ and the field $F(0)$ can be determined by J from the continuity equation $P(x) = P(0)$ and C is :

$$C = J[\frac{1}{q\mu P(0)}]^{\frac{l+1}{l}}(\frac{\epsilon_r\epsilon_0}{qH_b})(\frac{l}{l+1})(q\mu N_V)\frac{1}{l} \tag{1.20}$$

where $P(0) \approx N_0 \exp(\frac{-\phi_B}{k_B T})$ and N_0 is the density of electrons at the Fermi level of metal electrode.

If we look at Eq.1.19, we can see that two interesting boundary cases can arise. Firstly, when C is much more smaller than d, then C can be neglected and we get the Eq.1.17. If C cannot be neglected compared to d, $J - V$ curves deviate from the SCLC power law.

Secondly, we assume that $C > d$. After expanding the denominator in Eq.1.19 by binomial expansion, one can obtain

$$J = q\mu P(0)\frac{V}{d}(1 + \frac{l}{(2l+1)}\frac{d}{C})^{-1} \tag{1.21}$$

For $C \gg d$, the second part in Eq.1.21 can be neglected and we have

$$J = q\mu P(0)\frac{V}{h} \tag{1.22}$$

This result shows that for finite (non-zero) Schottky barrier (large value of C and $P(0) < \infty$) the current changes from the SCLC to ohmic current.

The whole topic of finite Schottky barrier is in great detail discussed in Ref.[25].

1.7 Temperature dependence of $J(V)$ characteristics

"The assumptions and approximations used in deriving Eq. 1.17 break down at low temperatures or at high-applied voltages. At room temperature and at low applied voltage the values of $J(V)$ obtained using this equation agree closely with the numerical solutions. Eq. 1.17 should also yield Arrhenius straight lines if log I values are plotted as a function of $1/T$. " [21]

According to Ref.[21], after some algebraic operations, Eq. 1.17 can be rewritten as

$$J = (\frac{\mu N_V q V}{d}) f(l) \exp[-\frac{E_t}{kT}\ln(\frac{qH_b d^2}{2\epsilon_r\epsilon_0 V})] \tag{1.23}$$

where

$$f(l) = (\frac{2l+1}{l+1})^{l+1}(\frac{l}{l+1})^l \frac{1}{2^l} \tag{1.24}$$

In practice, l is always more than 2 and we obtain

$$J = \left(\frac{\mu N_V q V}{2h}\right) \exp[-\frac{E_t}{k_B T}\ln(\frac{qH_b h^2}{2\epsilon_r\epsilon_0 V})] \tag{1.25}$$

Eq. 1.25 predicts that the plot $\ln J$ vs $1/T$ will be straight line (Arrhenius type). But the activation energy obtained from the slope of this line is not the activation energy E_t but this energy is multiplied by a factor γ :

$$\gamma = \ln(\frac{qH_b h^2}{2\epsilon_r\epsilon_0 V}) \tag{1.26}$$

Therefore we obtain effective activation energy given by relation

$$E_{t(eff)} = \gamma E_t \tag{1.27}$$

The effective activation energy can be observed experimentally and it is a function of applied voltage V and the trap density H_b. [21]

1.8 Carrier tunneling

Slight temperature dependence is a characteristic property of the carrier tunneling.

The Fowler-Nordheim model for tunneling injection (field emission) invokes tunneling of electrons from the metal through a triangular barrier into unbound continuum states. If the field emission dominates, the $J-V$ characteristics are described by equation ([10]):

$$J = (\frac{q^3}{8\pi\varphi\varsigma})F^2 \exp(-\frac{8\pi\sqrt{2m^*\varphi^{3/2}}}{3q\varsigma F}) \tag{1.28}$$

where φ is the barrier height between the electrode and the polymer film, m_h^* is the effective mass of the carriers and ς is the Planck constant.
For fitting the Fowler-Nordheim tunneling theory to the obtained data, the relation given by Eq. 1.28 changes to

$$I \propto F^2 \exp(\frac{-\kappa}{F}) \tag{1.29}$$

where I is the current, F is the electric-field strength and κ is a parameter which depends on the barrier shape. At high applied fields, the curves given by relation 1.29 are straight and from their slope, one can obtain the parameter κ.
The constant κ is then given by relation ([38])

$$\kappa = \frac{8\pi\varphi^{3/2}\sqrt{2m_h^*}}{3q\varsigma} = constant \tag{1.30}$$

From Eq. 1.30 the barrier height can be estimated by relation

$$\varphi = [\frac{3\kappa q\varsigma}{8\pi\sqrt{2m^*}}]^{2/3} \tag{1.31}$$

The barrier height φ is defined as the energy gap between the HOMO (or LUMO) of the polymer and the respective electrode work function and it can slightly vary with temperature. [10]

It was shown ([38, 10]) that in cases of some of the polymer devices, the $I-V$ characteristics are only slightly dependent on the field and temperature (example in Fig.1.6).

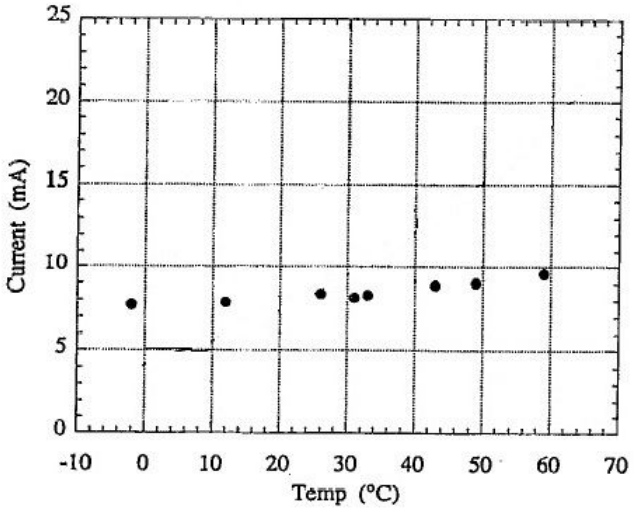

Figure 1.6: The current temperature dependence of a ITO/MEH-PPV/Au device operating at $17V$ bias [38]

1.9 Hopping conduction

Hopping conduction is present in different situations when band conduction does not occur. It is possible to move charge between localised states by thermal excitation. In these situations, electron has to jump across an energy barrier and also move in space from one site to another site. An electron may either hop over or tunnel through the barrier (Fig.1.7).

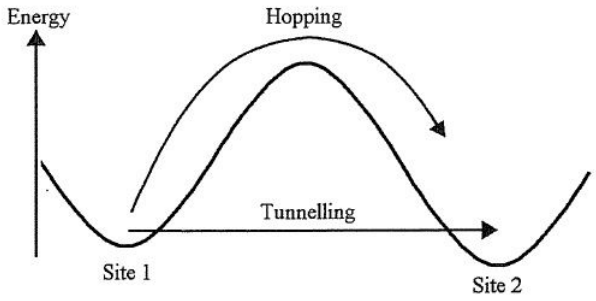

Figure 1.7: Schematic diagram of electron-transfer mechanisms between two sites separated by a potential-energy barrier [4]

If the electron jumps between the sites, it must get sufficient thermal energy to surmount the barrier. But for tunneling, the site separation has to be small enough for the tail of the electron wave function to widen over the barrier.

When the density of structural defects increases, the Fermi level will take place in the distribution of defect states and tunneling or thermally assisted hopping will become possible. The energetic and spatial distributions of states are affected by increasing disorder

in the lattice. For a random distribution of atoms in the material, the energy states spread as a tail into band gap and electrons in these states are localised (see Fig.1.8).

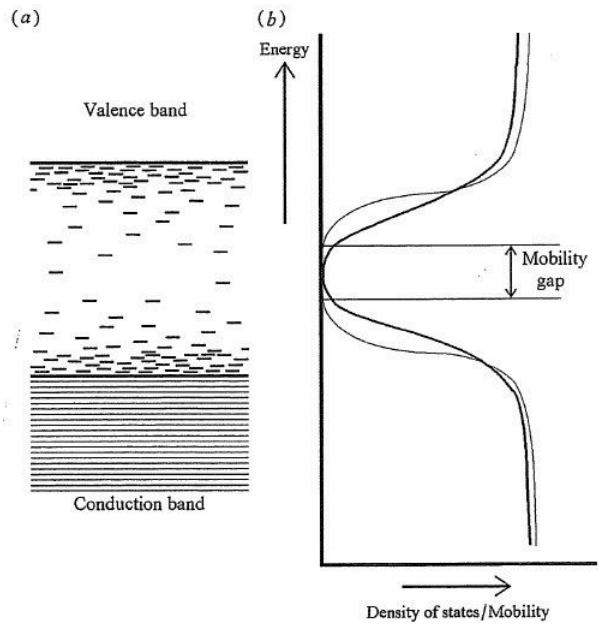

Figure 1.8: Defect states in a partially disordered semiconductor (a) and density of states (thicker line) and the mobility (thin line) of a disordered material (b) [8]

The localisation in the material connected with a disorder affects the mobility of charges. Hopping mobility falls off rapidly with hopping distance, so there is more mobility gap than the energy gap (Fig.1.8).

If the Fermi level is situated above the mobility edge, the electron wave functions are delocalised and the transport is possible. In this situation, the material is metallic.

But when the Fermi level lies below the mobility edge the electrons are localised and the material behaves like an insulator. In this second case conduction can occur by either :

a) thermal excitation from the Fermi energy level to the mobility edge when the conductivity is thermally activated with a well-defined activation energy :

$$\sigma = \sigma_0 \exp(-\frac{E_m - E_F}{k_B T}) \tag{1.32}$$

where E_m is the energy of the mobility edge or

b) by thermally activated hopping when the density of states within localised levels at the Fermi energy is non-zero

Situation a) will dominate at high temperatures and b) will dominate if the thermal energy is insufficient to excite electrons above the mobility edge.

If the range of the hops increases, the greater is the probability of the electron to find a site with a small energy barrier and these long-range hops depend on the extent of the tails of the electron wavefunctions. This behaviour has a characteristic temperature dependence

significant for the variable range hopping. Temperature dependence for this case differs from the Arrhenius law, which is usually anticipated for the thermally activated processes.

The hopping probability Φ (and the conduction σ too) has the form

$$\Phi = A \exp(-\frac{B}{T^n}) \tag{1.33}$$

where n is a number between one half and one quarter, A and B are constants.

Variable-range hopping (VRH) is discussed in the literature. Theoretical method for the description of VRH in Gaussian DOS by the percolation approach is shown in Ref. [2].

1.10 Mobility model

There are several approaches how to describe mobility in disordered organic semiconductors.

The Poole-Frenkel (PF) model was one of the first models which described electron-field dependence of the charge carrier mobilities. The field-dependent mobility can be given by relation

$$\mu = \mu_0 \exp(\beta_{PF}\sqrt{F}) \tag{1.34}$$

where μ_0 is the zero-field mobility and PF slope β_{PF} is

$$\beta_{PF} = \sqrt{\frac{q^3}{\pi\epsilon}} \tag{1.35}$$

The problem is that the Poole-Frenkel model does not involve temperature dependence in Eq.1.34. It is believed that the better way to describe the mobility in disordered organic semiconductors is the Gaussian disorder model (GDM). This model is based on the concept that the charge hopping in an amorphous material takes place between sites whose energy and spatial distribution is Gaussian. Charge hopping is thermally activated and field assisted so the mobility depends both on electric field F and temperature T. The mobility in the GDM is then described by equations

$$\mu(F,T) = \mu_\infty \exp[(-\frac{2\Lambda}{3k_BT})^2] \exp(\beta\sqrt{F}) \tag{1.36}$$

where

$$\beta = C[(\frac{\Lambda}{k_BT})^2 - \Sigma^2] \tag{1.37}$$

Σ is the geometric randomness and $\Lambda$is the energetic disorder which can be known as the width of the Gaussian distribution of the density of energy states for the transport sites and μ_∞ is the high temperature limit of the mobility. [45]

Theoretical discussion about temperature dependence in disordered organic solids can be found in Ref.[1].

2 Role of excitons in polymers

Very important factors which are base for use of the polymers in optoelectronics (OLED, organic solar cells or various detectors), are exciton formation and dissociation. These factors are concisely described in the following part together with the experimental method which is able to evaluate important transport parameters of exciton effects in polymer layers.

2.1 Exciton formation and dissociation

In organic materials, the excitons are created after the absorption of light. Exciton can be considered either as a neutral excited state of a molecule or as an electron-hole pair, bound together by Coulomb and lattice interactions ([14]). In the appropriate devices exciton dissociation occurs ([30, 13]). The transport of charges is affected by recombination during the journey to the electrodes. Interactions with atoms or other charges can slow down the travel speed and limit the current. [36]

2.2 Surface Photovoltage Method

The surface photovoltage method is a contactless method which is used mainly to determine the important transport parameter, namely the exciton diffusion length in semiconducting layers. This method, which originally comes from Goodman ([12]), was rearranged for measuring of thin layers (as polymers are).

The surface photovoltage (SPV) in a polymer layer is the result of dissociation of photogenerated free excitons in the electric field of the space charge region (SCR), which is formed in the sample. Used concept of the SPV calculates both currents from the bulk and currents from the SCR where recombination of charge carriers is considered.

Back to the history, a method for the measurement of the short minority carrier diffusion length in semiconductors was used by Alvin M. Goodman and applied to gallium arsenide. We want to show his approach here, citing the source [12] :

"The surface photovoltage ΔV developed at the illuminated surface is a function of the excess minority carrier density Δp injected into the surface space charge region. The density Δp is in turn dependent upon the incident light intensity I_0, the optical absorption coefficient α and the diffusion length L.

A steady state solution of the one dimensional diffusion equation for the sample geometry shown in Fig. 2.1 is

$$\Delta p = \frac{QI(1-\rho_1)}{(D/L)+s}\frac{\alpha L}{1+\alpha L} \tag{2.1}$$

assuming that $\alpha h \gg 1$, $\alpha l_1 \ll 1$, $h \gg L$, $l_1 \ll L$ and $\triangle p \ll n_0$.
Q is the photon quantum efficiency for hole-electron pair creation (inorganic semiconductors

are considered), ρ_1 is the optical reflection coefficient at the illuminated surface, s is the surface recombination velocity at the illuminated surface, h is the sample thickness and l_1 is the depth of the space charge layer at the illuminated surface. The relation (2.1) assumes that $\alpha h \gg 1$, consequently it holds for "thick samples".

The surface photovoltage may be written as

$$\Delta V = f[CI_0\alpha/(1+\alpha L)] \tag{2.2}$$

if ρ_1 and Q are essentially constant over the region α of interest, C is a constant and the form of functional dependence f needs not to be known explicitly.

It is a monotonic function and may therefore be inverted to obtain

$$I_0\alpha/(1+\alpha L) = F(\Delta V) \tag{2.3}$$

The same value of ΔV may be obtained for two different values of I_0 (perhaps $I_1$and I_2) provided that the corresponding values of λ and α (α_1 and α_2) are chosen. It follows from Eq. 2.3 :

$$I_1\alpha_1/(1+\alpha_1 L) = I_2\alpha_2/(1+\alpha_2 L) \tag{2.4}$$

Finally the diffusion length L may be obtained as : "

$$L = \frac{I_2\alpha_2 - I_1\alpha_1}{\alpha_1\alpha_2(I_1 - I_2)} \tag{2.5}$$

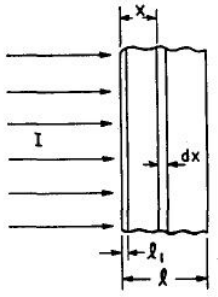

Figure 2.1: Sample geometry : I is the incident photon flux, l_1 is the depth of the surface space-charge layer at the illuminated surface and l is the sample thickness ([12])

Disadvantage of the limitation to thick samples and the assumption of constant value of the reflection coefficient is removed in the following theory. This theory was applied to inorganic as well as organic materials ([46],[48],[49]).

The photovoltaic effect requires an electric field for dissociation of photogenerated excess carriers (excitons in the case of polymer materials), which can then lead to the generation of a photocurrent in an external circuit. We assume that such field is formed in the space

charge region (SCR) at ITO/semiconductor interface.

The model, which is used in the following text, is performed assuming a polymer layer with neutral bulk and one space charge region. After illumination, excitons are generated both in the bulk and in the SCR. The model considers that the bulk/SCR interface is the place where the charge separation of excitons generated in the bulk occurs. Bulk diffusion current is formed in this way. Drift current results from the excitons photogenerated in the SCR and dissociated by the field of this region.

The total photocurrent is a sum of the diffusion current from the bulk and the drift current from the SCR.

In the next paragraph we show the main equation which we use for description of SPV experiments.

The transport of excitons in the bulk is described by the diffusion equation

$$\frac{d^2\Delta n(x)}{dx^2} - \frac{\Delta n(x)}{L^2} = -\frac{g(x)}{D} \tag{2.6}$$

where $\Delta n(x)$ is the concentration of the excess excitons at depth x in the bulk, L is the exciton diffusion length and D is the exciton diffusion coefficient.

In the case of multiple reflections, neglecting interference effects, the photogeneration rate $g(x)$ can be expressed as

$$g(x) = \alpha(1-R_1)I_0\left(\frac{\exp(-\alpha x) + R_2[\exp(-\alpha(2h-x))]}{1 - R_1R_2\exp(-2\alpha h)}\right) \tag{2.7}$$

where I_0 is the photon flux density impinging on the polymer layer, α is the absorption coefficient, h is the total thickness of the layer and $R_1$is the reflectance from the illuminated surface and R_2 is the reflectance from the bottom surface. Illumination from the side of the bulk is assumed.

To find the photogenerated current, we need two boundary conditions :

at the free surface : $\frac{Dd\Delta n(x)}{dx} \mid_{x=0} = s\Delta n(0)$

at the bulk/SCR interface : $\Delta n(d) = 0$

Here d is the thickness of the bulk and s is the surface recombination velocity. The unit area of the illuminated surface is considered. The diffusion current J_b from the bulk is :

$$J_b = \frac{eDd\Delta n(x)}{dx} \mid_{x=d} =$$
$$-\frac{a_1\alpha L}{1-\alpha^2L^2}\left\{\frac{[(1-S)\exp(-d/L)-(1+S)\exp(d/L)]\exp(-\alpha d)+2(\alpha L+S)}{(1+S)\exp(d/L)+(1-S)\exp(-d/L)} - \alpha L\exp(-\alpha d)\right\}$$

$$+\frac{a_2\exp(-\alpha w)\alpha L}{1-\alpha^2L^2}\left\{\frac{(1+S)\exp(d/L)-(1-S)\exp(-d/L)+2(\alpha L-S)\exp(-\alpha d)}{(1+S)\exp(d/L)+(1-S)\exp(-d/L)}\right\} - \alpha L \tag{2.8}$$

where a_1 and a_2 are :

$$a_1 = \frac{eI_0(1-R_1)}{1-R_1R_2\exp(-2\alpha h)} \tag{2.9}$$

$$a_2 = \frac{eI_0(1-R_1)R_2\exp(-\alpha h)}{1-R_1R_2\exp(-2\alpha h)} \tag{2.10}$$

Total thickness h of the sample is the sum of thickness of bulk (d) and SCR (w) :

$$h = d + w \tag{2.11}$$

and S is the dimensionless parameter

$$S \equiv \frac{sL}{D} \tag{2.12}$$

The current density J_s , from the SCR, is given by integration of the exciton photogeneration rate over the thickness of the SCR :

$$J_s = a_1 G\exp(-\alpha d)\int_0^w \alpha\exp(-\alpha x)dx + a_2 G\int_0^w \alpha\exp(-\alpha x)dx = G(1-\exp(-\alpha w))[a_1\exp(-\alpha d)+a_2] \tag{2.13}$$

The factor G ($G\epsilon(0,1)$) represents recombination losses in the SCR.

In Ref.[49] it was shown that the currents J_b and J_s are independent.

Then the total photocurrent density is the sum of (2.8) and (2.13).

$$J = J_s + J_b \tag{2.14}$$

The experimentally verified linear relation between the photovoltage and the low light intensity leads to the proportionality between the photovoltage V and the total photogenerated current density J

$$V \sim J \tag{2.15}$$

3 Polymer layers with nanoparticles

The improvement of properties of the polymer layers with regard to the applications in organic devices is made by fabrication of the blend structures. The interesting possibility of preparing these structures is incorporating of inorganic nanoparticles into the polymer layers. In the last decade inorganic nanoparticles play important role especially in the preparation of inorganic-organic hybrid solar cells. In the following text we will show some properties of the hybrid structures.

3.1 Inorganic-organic hybrid solar cells

Bulk heterojunction solar cell is often made of polymer (p-type) and PCBM (n-type). The problem with expensive fullerenes is, that they have weak absorption in the visible spectral range (Fig.3.1). In this case, one component of the photoactive blend is almost optically inactive. To overcome this limitation, alternative electron acceptors that are capable of absorbing visible light preferably at the lower energy part of the spectra are required. Moreover, the strong optical absorption needs to be accompanied by efficient electron transport. One option which can solve these problems is a hybrid solar cell.

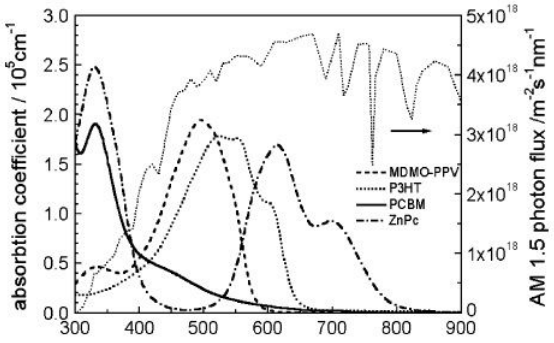

Figure 3.1: Absorption coefficients of layers of commonly used materials are shown in comparison with the standard AM 1.5 terrestrial solar spectrum [13]

A hybrid solar cell consists of a combination of both organic and inorganic semiconducting materials. It combines the unique properties of inorganic semiconductors with the film-forming properties of the conjugated polymers.

Organic materials are usually inexpensive, easily processable and their functionality can be tailored by molecular design and chemical synthesis. Inorganic semiconductors can also be manufactured as processable nanoparticulate colloids. By varying the size of the nanoparticles, their band gap can be tuned and their absorption/emission spectra can be tailored.

An effective strategy for hybrid solar cell fabrication is to use blends of nanocrystals with semiconductive polymers as bulk heterojunction. Excitons created upon photoexcitation are separated into free charge carriers very efficiently at interfaces between organic semiconductors and inorganic semiconductor nanoparticles in a hybrid composite thin film. Hybrid solar cells have been demonstrated in conjugated polymer blends containing CdSe, CdS or PbS nanoparticles.

Ideal structure of hybrid solar cell is presented in Fig. 3.2. This structure represents two main goals which one needs to achieve in the case of efficient hybrid organic solar cell. Firstly, there should be large interface area between organic and anorganic material. Around this interface, excitons can be dissociated. Secondly, we need pathway for both electrons and holes after dissociation to proper electrodes.

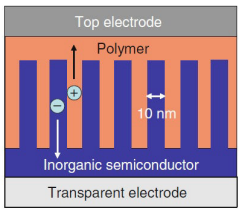

Figure 3.2: Ideal structure of hybrid organic solar cell [32]

The nano-sized particles exhibit unique properties different from that of the bulk semiconductor. When these inorganic nanoparticles are mixed in a semiconducting conjugated polymer host, a photovoltaic device (hybrid solar cell) can be fabricated with external quantum efficiency of 60%.

The usage of inorganic semiconductor nanoparticles embedded into semiconducting polymer layers is promising for several reasons :

(1) Inorganic semiconductor nanoparticles can have higher photoconductivity as compared to many organic semiconductor materials

(2) The p- or n-type character of nanocrystals can be varied by synthetic routes.

(3) Band gap of inorganic nanoparticles is a function of nanoparticle size. If the inorganic nanoparticles become smaller than the size of the exciton in the bulk semiconductor (usually about 10 nm), the electronic structure of such small particles is more like those of giant molecules than an extended solid. The electronic and optical properties of such small particles depend not only on the material of which they are composed, but also on their size. [34, 13]

More detailed discussions about hybrid solar cells and about suitable materials and fabrication techniques can be found in Ref. [32, 5].

3.2 Nanoparticle properties

Most of the following text comes from Ref. [42].

Semiconductor materials have very promising property, because they exhibit the same physical properties irrespective of their size above a particular value called the threshold value for each material. Below this threshold, the band gap of the semiconductor materials increases with a decrease in their size.

Nanoparticles are usually defined according to their size. Particles with size more than 1 nm and less than or comparable to 100 nm are classified as nanoparticles. Quantum dots are referred to as nanoparticles in the case of semiconductors which have quantum-confinement property. Nanoclusters are also nanoparticles whose size lies between 1 and 10 nm with a narrow size distribution which always show the effect of the quantum confinement (detailed discussion about different quantum properties of quantum dots can be found in Ref. [3]).

Size dependence of band gap for CdS material is shown in Fig. 3.3.

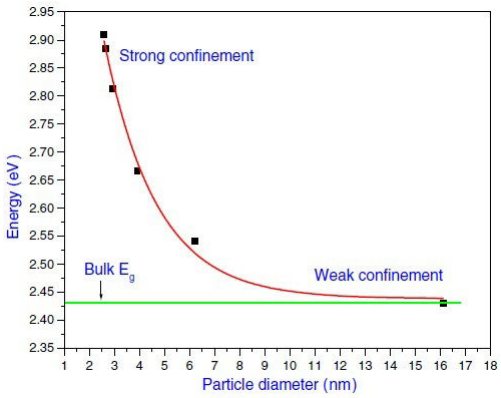

Figure 3.3: Size dependence of band gap for CdS nanoparticles [52]

The absorption peak corresponding to the threshold for the absorption of light in the quantum dot is blue-shifted with decreasing size (as compared with the bulk material).

According to the effective mass approximation, the energy band gap of nanoparticles (E_{nano}) showing a quantum confinement effect is related to the band gap of bulk material as

$$E_{nano} = E_g + \frac{\pi^2\hbar^2}{2r^2}(\frac{1}{m_e^*} + \frac{1}{m_h^*}) \tag{3.1}$$

where E_g is the band gap of bulk material, r is the radius of the nanoparticels showing the quantum confinement effect and $m_e^*(m_h^*)$ is the effective mass of the electron (hole).

In semiconductors, the optical spectra may have photon energies less than that of the band gap due to the excitonic recombination. If we consider the case of free excitons (Mott-Wanier excitons), then the electron and the hole are attracted each other via the Coulomb potential and it is

$$V(r) = -\frac{q^2}{4\pi\epsilon_0\epsilon_r r} \tag{3.2}$$

where ε is the dielectric constant and r is the distance between the electron-hole pair.

The Hamiltonian of an exciton confined to a nanoparticle of radius r can be written as

$$H = \frac{p_e^2}{2m_e^*} + \frac{p_h^2}{2m_h^*} - \frac{q^2}{k_w \|\overrightarrow{r_e} - \overrightarrow{r_h}\|} \tag{3.3}$$

where $p_{e,h}$,$\overrightarrow{r_{e,h}}$ and $m_{e,h}^*$ are the momentum, coordinate and the effective mass of the electron or hole and k_w is the wave vector.

The following expression was derived for the exciton energy :

$$E_{ex} = E_g + \frac{\hbar^2\pi^2}{2r^2}(\frac{1}{m_e^*} + \frac{1}{m_h^*}) - \frac{1.786q^2}{4\pi\epsilon_0\epsilon_r r} - 0.248\frac{\varpi q^4}{2\hbar^2(4\pi\epsilon_0\epsilon_r)^2} \tag{3.4}$$

We can rewrite it by using Eq.3.1 like

$$E_{ex} = E_{nano} - \frac{1.786q^2}{4\pi\epsilon_0\epsilon_r r} - 0.248\frac{\varpi q^4}{2\hbar^2(4\pi\epsilon_0\epsilon_r)^2} \tag{3.5}$$

where ϖ is the reduced effective mass

$$\varpi = \frac{1}{\frac{1}{m_e^*} + \frac{1}{m_h^*}} \tag{3.6}$$

In most references ([29, 7, 41]), Eq. 3.5 is reduced to this form :

$$E = E_g + \frac{\hbar^2\pi^2}{2r^2}(\frac{1}{m_e^*} + \frac{1}{m_h^*}) - \frac{1.8q^2}{4\pi\epsilon_0\epsilon_r r} \tag{3.7}$$

We can see (from Eq.3.5) that the exciton energy of the nanoparticles is dependent on the radius, it decreases with an increase of size.

The exciton energy obtained from Eq. 3.5 for spherical nanoparticles corresponds with the experimental results and it deviates in case of nonspherical nanoparticles.

3.3 ZnO and CdS nanoparticles

Zinc oxide (ZnO) is a $II - VI$ direct band-gap semiconductor material.

ZnO is one of the most promising candidates for the UV emitter applications due to its wide-band-gap of $\sim 3.3eV$ (at $300K$) and a high exciton binding energy of $60meV$.

More detailed work about ZnO material can be found in Ref. [22]. Interesting applications of ZnO material in hybrid solar cells are described in Ref. [44, 37].
Cadmium sulfide (CdS) is a direct band-gap semiconductor with $E_g \sim 2,48eV$ and it is a promising material for photoelectric conversion in solar cells and ligh-emitting diodes ([53]). The syntheses of CdS nanoparticles and investigation of CdS properties have become of much interest. Details can be found in Ref. [16, 52].

Part II

Experimental

4 Materials

4.1 Polymer materials

Several polymer materials were used for preparing samples for measurements in this thesis. Firstly, we used polymer called "MEH-PPV" but the original name is Poly[2-methoxy-5-(2-ethylhexyloxy)-1,4-phenylenevinylene]. Another polymer material was "PT" which means Polythiophene. Both of these materials are shown in Fig. 4.1.

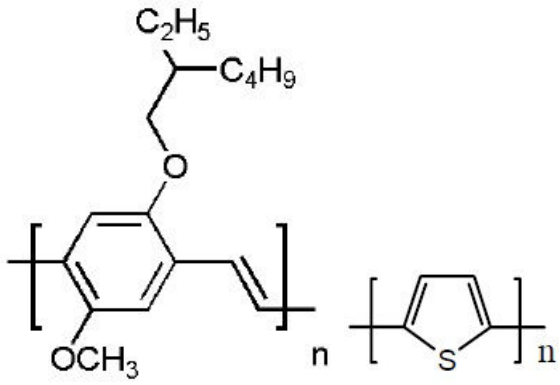

Figure 4.1: MEH-PPV (left [40]) and PT (right [9])

Another interesting material used in this work is PEDOT:PSS, its original name is Poly(3,4-ethylenedioxythiophene):Poly(styrenesulfonate). This material consists of two parts - Poly(3,4-ethylenedioxythiophene) (shown in upper part of Fig. 4.2) and Poly(styrenesulfonate) (see lower part of Fig. 4.2).

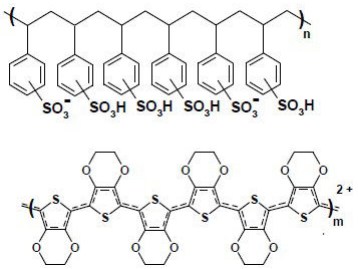

Figure 4.2: PEDOT:PSS (Sigma-Aldrich information)

4.2 Anorganic materials

CdS nanoparticles No. 662372 were purchased from the Sigma-Aldrich company. The company states that the nanoparticles with carboxylic acids used as the capping agent were organically stabilized in toluene and that their particle size is around $5nm$.

Two types of ZnO nanoparticles were used. One type (No. 721085) was purchased from the Sigma-Aldrich company as a solution in ethanol, $40wt\%$. Sigma-Aldrich states that the particle size is $< 130nm$.

Second type of ZnO material was also purchased from the Sigma-Aldrich company (No. 677450) but this material was nanopowder-like (particle size $< 50nm$). Since a solution was needed (because of deposition of ZnO nanoparticles on glass/ITO substrate and because of preparation of samples for TEM measurements), we prepared a solution from this nanopowder. The solution was made of $50mg$ Zno powder together with $0,25mL$ of methanol and $4,75mL$ of ethanol. After 30 minutes of sonification, the solution was prepared for deposition.

5 Film-Forming Techniques

Most of the samples measured and presented in this thesis were made by the spincoating method. Another method which was used for preparation of some measured samples was casting. These techniques are described in the following text, using Ref. [24] and Ref. [35]. All the MEH-PPV samples (also with CdS and ZnO nanoparticles) were prepared at Tomas Bata University in Zlin, Polythiophene samples were prepared at Department of Energy Conversion and Storage at Technical University of Denmark.

5.1 Spincoating

Perhaps the most important film-forming technique for the preparation of polymer layers is spincoating. In principal this method allows highly reproducible formation of films and it prepares very homogenous layers.

A typical spincoating procedure involves application of a liquid to a substrate followed by acceleration of the substrate to a selected rotational speed (see Fig. 5.1). Another option is application of the liquid solution while the substrate is spinning. The resulting thickness, morphology and surface topography depend strongly on rotational speed, viscosity, volatility, diffusivity, molecular weight and concentration of the solutes. They depend little on the amount of solution, the rate of deposition and the spinning time.

The film thickness h, obtained during a spincoating process is controlled by the empirical equation

$$h = z\omega^u \tag{5.1}$$

where ω is the angular velocity and z and u are empirical constants, which are related to the physical properties of the solvent, solute and substrate.

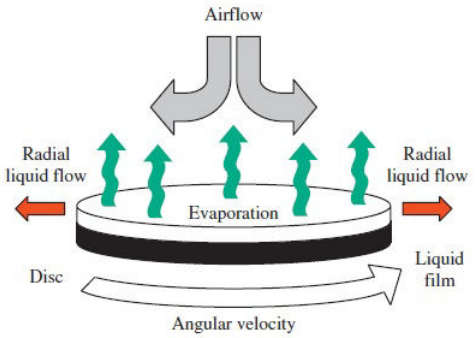

Figure 5.1: Schematic illustration of the spincoating processes [24]

5.2 Casting

This simple method needs virtually no special equipment. The procedure of film-making is really simple - the solution is cast onto a substrate and then the substrate is dried. The obvious disadvantage of this method is lack of control over the film thickness and picture framing effects are often seen near the edges of the layer. On the other hand, casting is a very simple method that consumes little time and it can be used for preparation of the samples if we do not need very homogenous and well-defined layer.

6 Preparation of samples for measuring of dark J-V characteristics

For making samples for dark J-V measurement, we used the following method.

Firstly, glass/ITO substrate was chemically treated and ITO layer was removed, except for two vertical stripes. After this treatment, polymer layer was spincoated onto the whole substrate and finally, three aluminium horizontal stripes were vacuum evaporated.

By this process, we obtained six samples on one substrate and we were able to put contacts onto aluminium and ITO stripes without touching the measured layer.

Measured samples are the places where the ITO and aluminium stripes cross each other. Substrate after using the discussed method is shown in Fig. 6.1. Schemes of resulting polymer layers can be seen in Fig. 6.2.

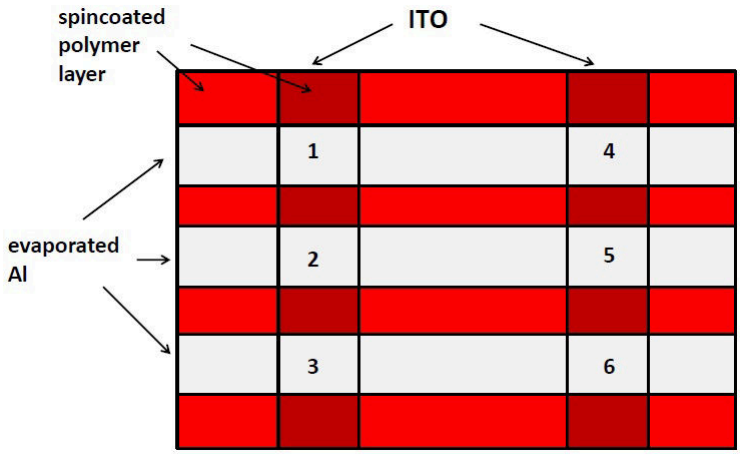

Figure 6.1: Adapted substrate for dark I-V measurement. Solution with polymer material was spincoated onto the whole substrate (red). Two ITO vertical stripes (dark red) were left after chemical treatment, so six samples (squares with numbers 1 to 5) arised after evaporation of alluminium horizontal stripes (grey).

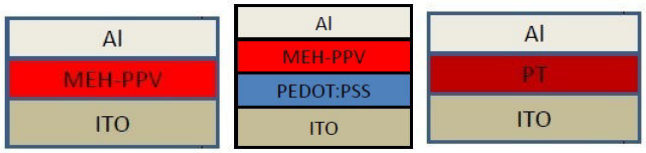

Figure 6.2: Scheme of samples for measurement of dark I-V characteristics. ITO/MEH-PPV/Al (left), ITO/PEDOT/MEH-PPV/Al (in the middle) and ITO/PT/Al (right)

7 Preparation of samples for SPV measurement

Several samples for SPV measurement were prepared. The spincoating technique was used for the preparation of thin polymer films where polymer materials MEH-PPV and PT played the main part. A scheme of prepared layers can be found in Fig.7.1 .

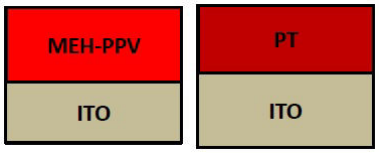

Figure 7.1: Samples for SPV measurement - MEH-PPV (left) and PT (right)

8 Preparation of samples containing nanoparticles

8.1 Samples for SPV measurement and UV-Vis Absorption Spectroscopy measurement

The sample of CdS nanoparticles for measurement of photovoltage was prepared by the following process : the suspension with CdS nanoparticles was cast on ITO covered glass electrode. The layer was dried at $85°C$ and because of a thicker surfactant, the layer needed to be measured in an electrochemical cell (instead of Mylar sheet). An iodine containing electrolyte was put between the glass/ITO electrodes, improving the charge transport.

Samples consisting of ZnO nanoparticles (both types) were prepared by a similar process as the CdS nanoparticles. The solution containing ZnO nanoparticles was cast on glass/ITO substrate and then dried at $85°C$ for 30 minutes. The layers also needed to be measured in an electrochemical cell so a drop of the electrolyte was placed between the glass/ITO electrodes.

Samples for UV-Vis Absorption Spectroscopy measurement were prepared by a similar method as for the SPV measurement. Only the improving of the charge transport was not needed so we did not prepare electrochemical cells.

8.2 Samples containing both polymer and inorganic material

Two methods for preparing hybrid layers (polymer layers containing inorganic particles) were used.

First method consisted of spincoating of ZnO solution onto glass/ITO substrate. After deposition, this layer was dried in vacuum. Polymer MEH-PPV was then deposited by the spincoating technique on glass/ITO/Zno layer. The resulting layer is shown in Fig. 8.1 on the right side. We believe that the MEH-PPV layer penetrated into the ZnO layer and simple hybrid layer arosed. We call this sample "porous" sample.

The second method was very simple - solution of MEH-PPV was mixed with a solution containing inorganic nanoparticles and the resulting solution was spincoated onto glass/ITO substrate. Layers made by this method are shown in Fig. 8.1 - a layer containing CdS nanoparticles (left) and a layer containing ZnO nanoparticles (in the middle). This sample is called "dispersive" sample. In the series, ITO/PEDOT/MEH-PPV+CdS sample was also made (see Fig. 8.1).

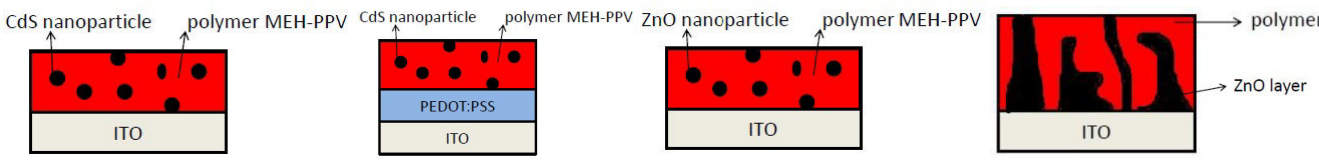

Figure 8.1: Different samples for SPV and UV-Vis Absorption Spectroscopy measurement containing both polymer material and inorganic nanoparticles

Part III

Experimental techniques

9 Surface Photovoltage Method (SPV) aparatus

The apparatus for SPV measurement is shown in Fig. 9.2. The photovoltage measurements were performed in a sandwich structure between two ITO electrodes with a Mylar sheet at the film surface serving as a dielectric layer (Fig. 9.1). A capacitive couple is formed in this way.

The sample was illuminated by low-intensity monochromatic light chopped with a low frequency of 11 Hz generating an alternating voltage which was measured between a transparent conductive electrode capacitively coupled to the sample and an appropriate back electrode by lock-in amplifier SSR 830.

The SPV spectra were taken at room temperature and in air. Maximum values of the photovoltage were $20 - 30\mu V$.

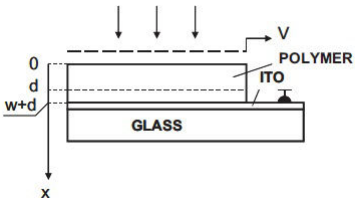

Figure 9.1: Sample arrangement for SPV contactless measurements - illuminated glass/ITO top electrode (dashed line) is separated from the polymer layer by Mylar film

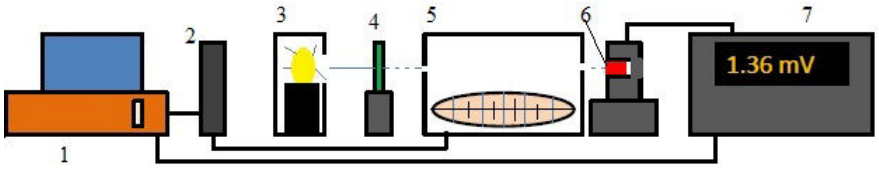

Figure 9.2: Scheme of experimental setup for SPV measurement : 1 is computer, 2 is automatic stepper motor, 3 is source of illumination, 4 is chopper, 5 is monochromator, 6 is sample and 7 is lock-in amplifier.

10 Ultraviolent and Visible (UV-Vis) Absorption Spectroscopy

"UV-Vis Absorption Spectroscopy is a very important, useful and easy analytical method. This method involves passing a monochromatic beam of light through a measured sample and then measuring the absorption wavelength of the material. When the photons pass through the material, it is possible that photons of a suitable energy interact with the material and electron can be excited to a higher energy state and the photon is being

absorbed. By measuring the amount of light absorbed for a particular wavelength, it is possible to deduce information about the electronic structure of the material. In conjugated polymers, UV-Vis absorption is due to $\pi - \pi^*$ transitions." [31]

Transmittance during our experiments was measured on different samples by Hitachi U-3300 Spectrophotometer. Measurements of all the samples were made in air.

11 Transmission electron microscopy (TEM) investigation

"In the transmission electron microscopy, a sample is bombarded with a finely focused beam of monochromatic electrons. Products of the interaction of the incident electron beam with the sample are detected. If the sample is sufficiently thin (up to $200nm$ thickness) the beam is transmitted after interacting with sample." [6]

Taking images from the transmission electron microscopy (TEM) in our case was performed on a transmission electron microscope Jeol 2000 FX. Main parameter - accelerating voltage - of this microscope is $200kV$.

12 Measuring of dark J-V characteristics

Dark J-V characteristics were measured by Keithley 2420 3A SourceMeter (it was the source of the voltage and an amperemeter, too). Measured data processing was done by the computer and because we measured J-V characteristics in different temperatures, cryostat with liquid nitrogen was used. The measurements were done in the vacuum which was achieved by the rotary pump.

Part IV

Results and discussions

13 Dark J-V characteristics measurement

We measured dark J-V characteristics on several polymer layers at different temperatures in the "hole-only" regime. In this regime ITO electrodes served as hole-injecting electrodes and Al electrodes served as a barrier for injecting of electrons whose concentration is denoted as p_0 (see Fig. 1.2).

Several parametres can be obtained from the measurements.

Very important parameter which describes the polymer material is the effective density of states (in the valence band, in our case) N_v which is given by relation

$$N_v = 2(\frac{2\pi m_h^* k_B T}{\varsigma^2})^{3/2} \tag{13.1}$$

Assuming the SCLC model for conduction in measured layer, the Ohmic region can be present in the J-V characteristic at low applied voltage, which corresponds to the current due to the background carriers (see Fig. 1.5). One can get mobility μ from Ohm´s law given as

$$J = q\mu p_0 \frac{V}{h} \tag{13.2}$$

where concentration of free holes p_0 is given by relation

$$p_0 = N_v \exp(\frac{-E_f - E_g}{k_B T}) \tag{13.3}$$

where E_f is the position of the Fermi level in the band gap and E_g is the value of the band gap.

If the SCLC model is assumed, for higher applied voltage the J-V characteristics obey the law given by Eq. 1.17 (assuming exponential distribution of traps).

13.1 MEH-PPV layers

Firstly, we would show scheme of the energy levels in the measured MEH-PPV samples (see Fig. 13.1). HOMO and LUMO levels positions are taken from Ref. [50] and position of the Fermi level was obtained from the Kelvin probe force microscopy.

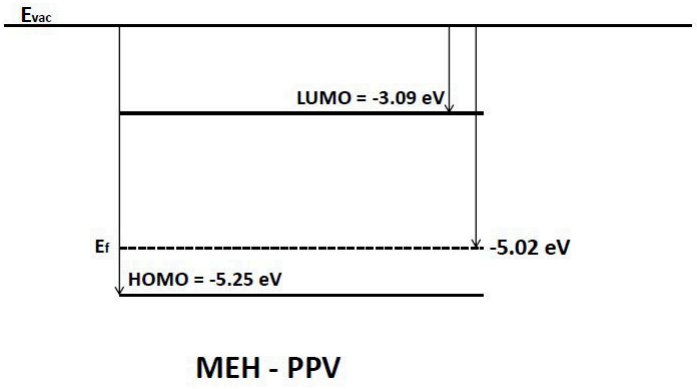

Figure 13.1: Scheme of energy levels in measured MEH-PPV samples

Measurement of dark J-V characteristic of ITO/MEH-PPV/Al sample at room temperature is shown in Fig. 13.2. Measured J-V characteristics of ITO/MEH-PPV/Al samples can be evaluated by the SCLC model. One can see the Ohmic region at the curve in Fig. 13.2 at low applied voltages and at higher voltages, the slope of the curve is 3.9. This should indicate behaviour predicted by Eq. 1.17 and presence of traps. Between Ohmic region and the region with the higher increase of the current density, we can see the transition region (similar behavior is shown in Fig. 1.5).

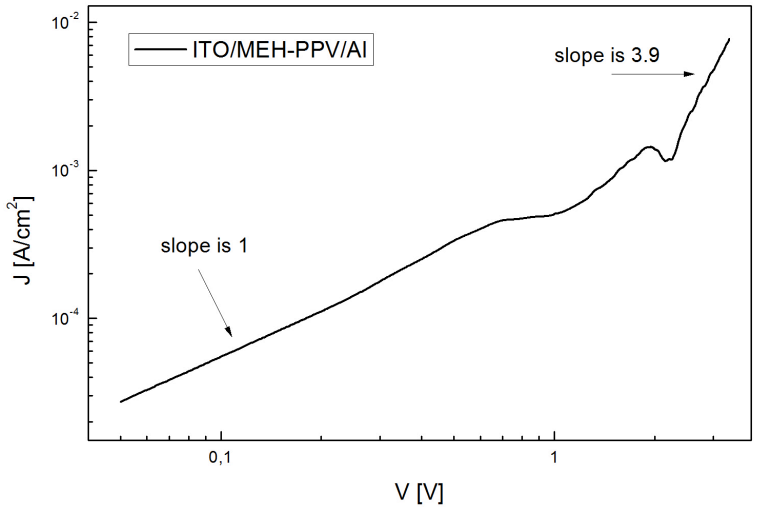

Figure 13.2: Dark J-V characteristic measurement of ITO/MEH-PPV/Al sample at room temperature

Two measurements at room temperature showing Ohmic regions are displayed in Fig. 13.3.

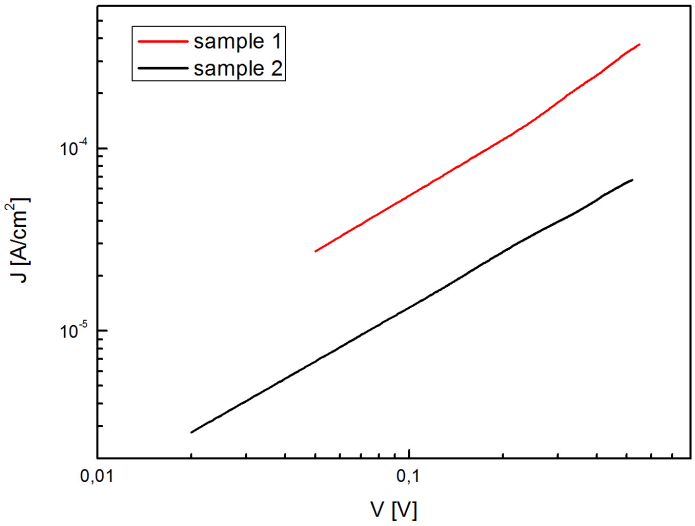

Figure 13.3: Ohmic region in dark J-V characteristics for two ITO/MEH-PPV/Al samples at room temperature

Using voltage and current density from the Ohmic region, we can get the hole mobility at room temperature using Eq. 13.2. Density of states for MEH-PPV is usually known as $N_v = 3.10^{19} cm^{-3}$ ([47, 21, 23]) and p_0 obtained from Eq. 13.3 for given parametres is $p_0 = 4,1.10^{15} cm^{-3}$ at room temperature.
The total thickness h of the MEH-PPV layers was measured by the ellipsometry measurement and was evaluated as $h = (40 \pm 4) nm$. Values of the mobility in the Ohmic region for two ITO/MEH-PPV/Al samples are shown in Tab. 13.1.

sample	$\mu[cm^2 V^{-1} s^{-1}]$
sample 1	$3,4.10^{-6}$
sample 2	$8,2.10^{-7}$

Table 13.1: Values of the mobility μ obtained from the Ohmic region of ITO/MEH-PPV/Al samples

J-V characteristics of ITO/MEH-PPV/Al sample at several temperatures are shown in Fig. 13.4. At higher applied voltages the curves are getting closer to each other. This phenomenon is because of the slopes which are decreasing with increasing temperatures.

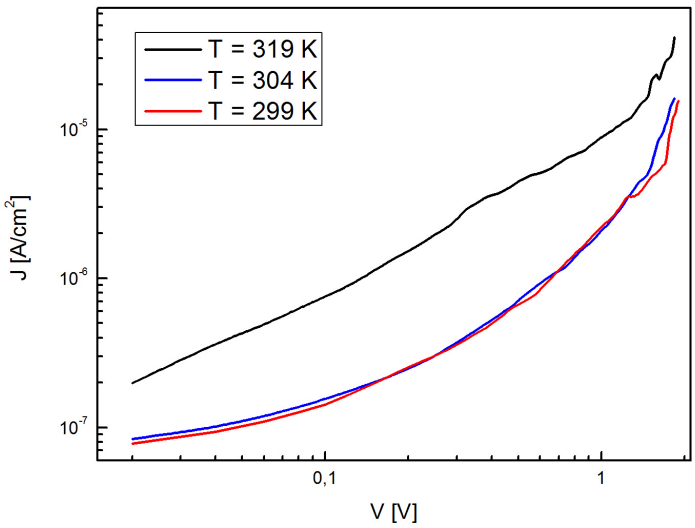

Figure 13.4: J-V characteristics of ITO/MEH-PPV/Al sample measured at three temperatures

Interesting way how to determine another important parameter - density of the traps H_b - is described in Ref. [26]. This method is quite simple - we need to extrapolate J-V characteristics (in log-log scale at two different temperatures) for higher voltages where power law is given by Eq. 1.17 for $l > 2$ to determine the cross over voltage V_C . This voltage is given as ([26]) :

$$V_C = \frac{qH_b h^2}{2\epsilon_r \epsilon_0} \tag{13.4}$$

By this method we evaluated two dark J-V characteristics ($T = 304K$ and $T = 319K$) at higher applied voltages. The cross over voltage was determined as $V_C = 2,75V$. Then we can obtain H_b from Eq. 13.4 as $H_b = 5,7.10^{17} cm^{-3}$. This value is similar to common values in the literature.

Dark J-V characteristics at different temperatures were also measured on ITO/PEDOT/MEH-PPV/Al samples. Results of these measurements are shown in Fig. 13.5.

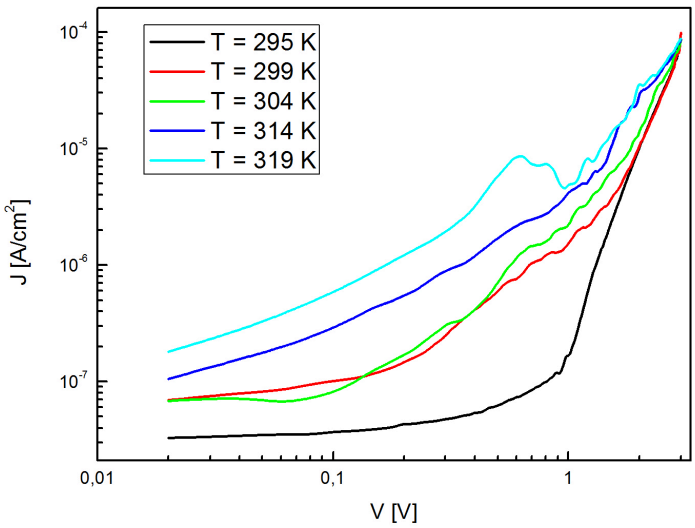

Figure 13.5: Measured dark J-V characteristics on ITO/PEDOT/MEH-PPV/Al sample at different temperatures

Shape of the measured curves is similar to prediction by the SCLC model. The characteristics are getting closer to each other at high applied voltage where slopes of the curves are higher.

Arrhenius plot taken at voltage $V = 2,5V$ is in Fig. 13.6. This lnJ vs $1/T$ plot is linear and there is only one activation energy in this region. We can obtain the slope of this plot which is proportional to the effective activation energy divided by k_B (Eq. 1.27). From Eq. 1.26 one can get the parameter H_b. We obtained density of the traps as $H_b = 3,8.10^{18} cm^{-3}$. This value is almost the same as refered in the literature ([47, 20, 27]) and it is a little bit higher than value obtained from the cross over voltage used for ITO/MEH-PPV/Al sample.

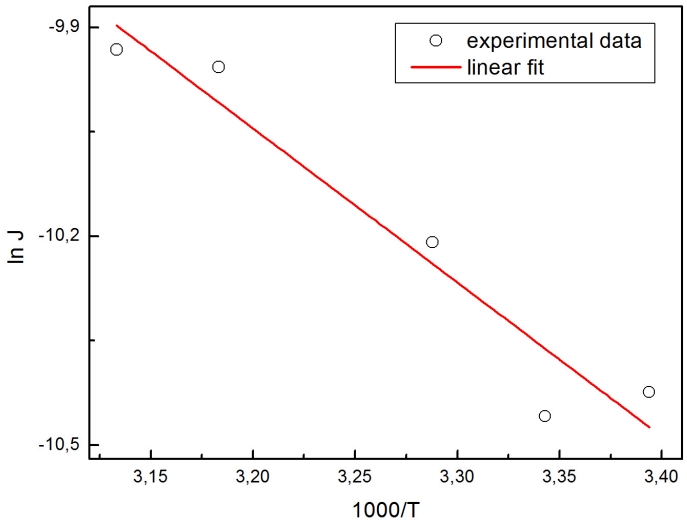

Figure 13.6: Arrhenius plot of the experimental data obtained from dark J-V characteristics at applied voltage $V = 2,5V$. Measured on ITO/PEDOT/MEH-PPV/Al sample

Assuming the SCLC model with the exponential distribution of the traps dark J-V characteristics at higher applied voltages are suitable for the evaluation of the mobility μ from Eq. 1.17 (especially if we have obtained parameter H_b). Resulting mobility from Eq. 1.17 at temperature $T = 299K$ for applied voltage $V = 2,5V$ is $\mu = 2,4.10^{-8} cm^2 V^{-1} s^{-1}$. This value is lower than mobilities obtained from the Ohmic region (see Tab. 13.1). Eq. 1.17 is very sensitive to change of parameters especially to the change of the slope of J-V characteristic. The small inaccuracy in the slope can lead to large inaccuracy in evaluation of other parameters, such as the mobility μ.

13.2 Polythiophene layers

Energy scheme of measured polythiophene is shown in Fig. 13.7. Positions of LUMO and HOMO levels were taken from Ref. [28] and the position of the Fermi level was obtained from the Kelvin probe force miscroscopy.

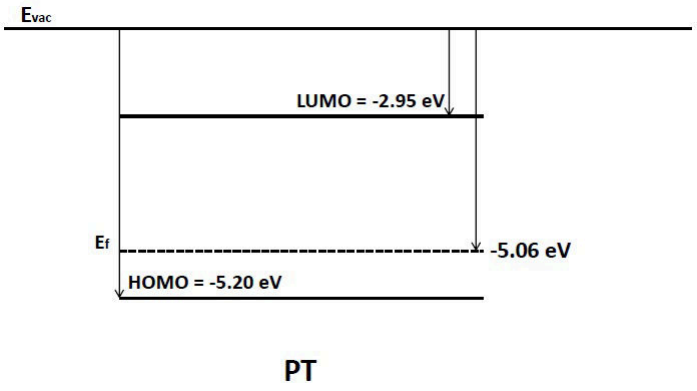

Figure 13.7: Scheme of energy levels in measured polythiophene (PT) samples

The hole effective mass m_h^* for Polythiophene is $m_h^* = 0.137m_e$ ([17]). According to Eq. 13.1 $N_V = 4,7.10^{17}cm^{-3}$ at room temperature and the background concentration of holes is then $p_0 = 1,7.10^{15}cm^{-3}$at room temperature.
Measured dark J-V characteristics on ITO/PT/Al sample at different temperatures are shown in Fig. 13.8. The total thickness h of the PT layers was measured by the ellipsometry measurement and was evaluated as $h = (40 \pm 4)nm$.

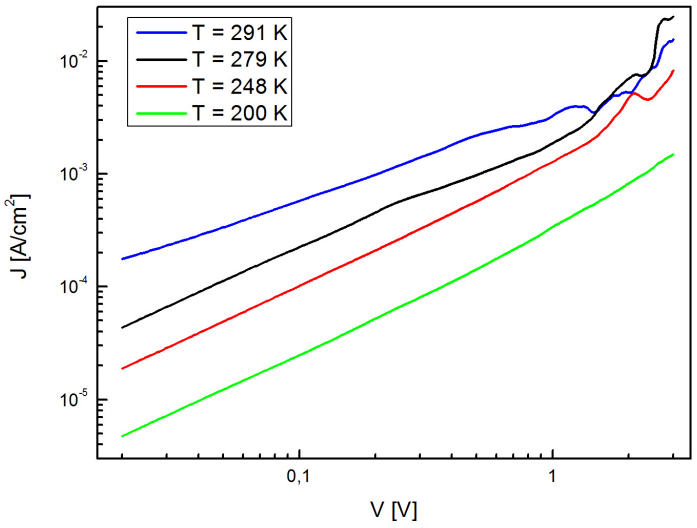

Figure 13.8: Dark J-V characteristics measured on the PT sample for different temperatures

The curves in Fig. 13.8 cross each other at high applied voltages and the slopes of the characteristics change with temperature and with the applied voltages. This strange behaviour is probably caused by the instability of the measured Polythiophene layers. The layers are very sensitive to the "history" of the measurement - it depends on the way how we heated the layer and it also depends on the applied electric field. All this factors

probably resulted in the behaviour which is displayed in Fig. 13.8 (especially at high applied voltages). Nevertheless measurements at higher voltages tend to show the possibility that the charge transport is controlled by the SCLC model.
The Ohmic region of measured characteristics is shown in Fig. 13.9. For temperature $T = 279K$ we obtain mobility from Eq. 13.2 as $\mu = 4,7.10^{-5} cm^2 V^{-1} s^{-1}$. Similar value can be found in the literature (Ref. [51]).

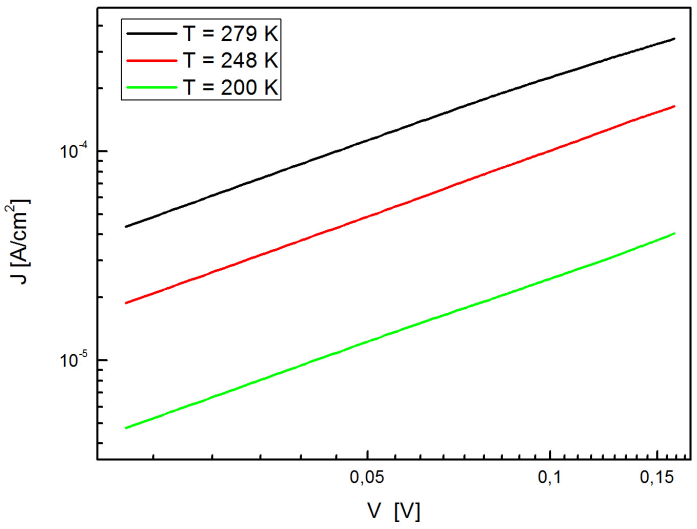

Figure 13.9: Ohmic region in measured dark J-V characteristics on PT sample for different temperatures

14 Theoretical photovoltage spectra

We have calculated surface photovoltage spectra according to Eq. (2.14). This equation contains several parameters, which describe different shape of theoretical curves. Perhaps the most important parameter which we can obtain from these curves is diffusion length L. The diffusion length L is therefore shown (as a parameter) in all photovoltage spectra (Fig.14.4-14.10). Other parameters also play important roles in the spectra and they will be described below.

We can see the absorption coefficient α in Fig.14.1 which is used for the spectra. The maximal coefficient α is for $\lambda = 480nm$. Reflectance R is shown on Fig.14.2. In the following calculations, we use only one reflectance, so $R = R_1 = R_2$. This approach is simplified and it will not be used during the evaluation of the experimental data.

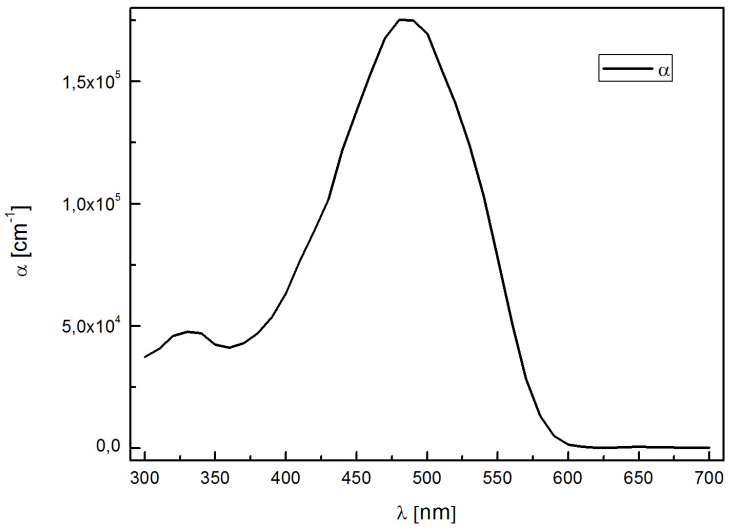

Figure 14.1: Spectral dependence of the absorption coefficient α used for the calculation of SPV spectra of MEH-PPV

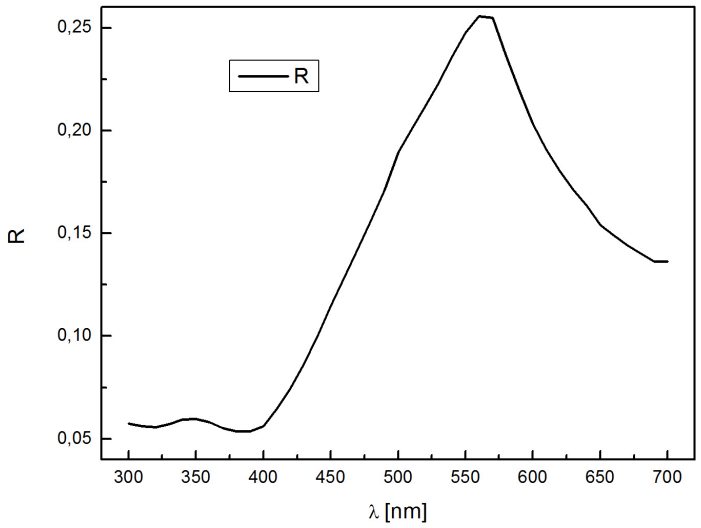

Figure 14.2: Reflectance used for the calculation of the photovoltage spectra for MEH-PPV

Some cases of possible photovoltage spectra are shown in the following text.

We chose four situations which are connected with different thickness of the SCR and of the bulk. These parameters are used for theoretical photovoltage spectra : $S = 1000$, $qI_0/J_0 = 1.10^{-3}$, $G = 0.01$ and $w + d = 150nm$. In the following text, we just change values of w and d (but the relation $w + d = 150nm$ is still valid) and the direction of the

incident radiation. Calculated photovoltage is normalized to the maximum value in the shown graphs.

First case is shown in Fig.14.4. Bulk is thick ($d = 130nm$), space charge region is thin ($w = 20nm$) and irradiation comes from the side of the SCR (scheme in Fig.14.3). The theoretical spectra for this case of illumination are derived in [49].

Main contribution to the measured voltage comes from the SCR. Shapes of the calculated photovoltage spectra are similar to the shape of the absorption coefficient α. Contribution from the bulk could be measured if excitons are created near the bulk/SCR interface. Curves in Fig. 14.4 are therefore almost independent on diffusion length L near the maximum of absorption but they are slightly dependent on the diffusion length in the regions of shorter and longer wavelengths. Near the maximum (around $480nm$) of the absorption, almost all excitons are created in the SCR or close to the SCR/bulk interface from the side of the bulk. But for other wavelengths, excitons are also created farther from the SCR/bulk interface from the side of the bulk. These excitons (created in larger distances from the SCR/bulk interface) also contribute to the photovoltage and their contribution is dependent on the diffusion length (as can be seen in Fig.14.4).

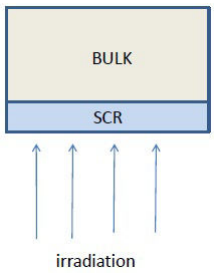

Figure 14.3: Scheme - thick bulk and thin SCR, illumination comes from the side of the SCR

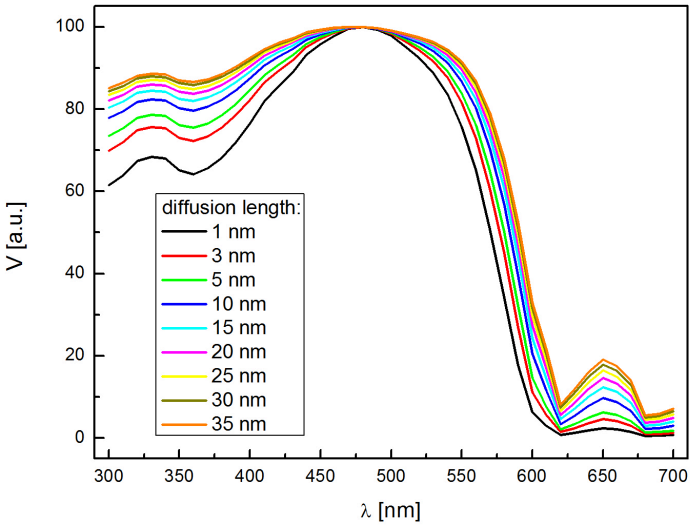

Figure 14.4: Photovoltage spectra -$w = 20nm$, $d = 130nm$ and light comes from the side of the SCR, $L \in < 1; 35 > nm$

Secondly, we assume that the bulk is thin ($d = 20nm$), the space charge region is thick ($w = 130nm$) and irradiation comes from the side of the bulk (Fig.14.6, scheme in Fig.14.5).

In this situation, the contribution comes from the bulk and from the SCR. Because the bulk is very thin, for almost all diffusion lengths the excitons are created near the bulk/SCR interface and they can be dissociated. The contribution from the SCR is bigger for shorter wavelengths because generation of excitons takes place closer to the bulk/SCR interface than for longer wavelengths.

The curves in Fig. 14.6 are therefore practically independent on diffusion length.

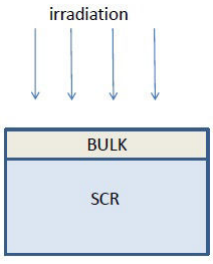

Figure 14.5: Scheme - thin bulk and thick SCR, illumination comes from the side of the bulk

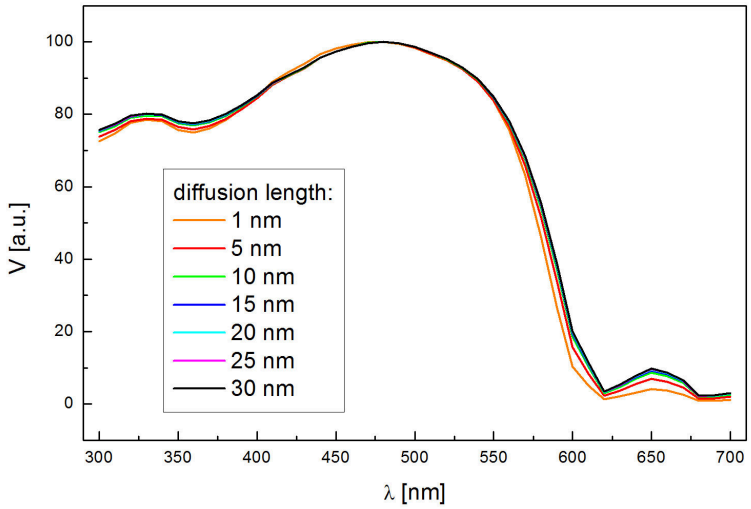

Figure 14.6: Photovoltage spectra - $w = 130nm$, $d = 20nm$ and light comes from the side of the bulk, $L \in < 1; 30 > nm$

Third case is shown in Fig.14.8. The bulk is thin ($d = 20nm$),the space charge region is thick ($w = 130nm$) and irradiation comes from the side of the SCR (scheme in Fig.14.7).

Around the maximum of the absorption, excitons are generated mostly in the SCR and the measured signal is small (it can be seen on the local minimum in Fig. 14.8 for $\lambda \backsim 480nm$) and dependent on the diffusion length. For wavelengths with smaller absorption some photons can get to the bulk and then the excitons are also generated in the bulk. With larger diffusion length, the signal is bigger because the excitons can get to the bulk/SCR interface easily. Nice example of this behaviour is the red curve ($L = 30nm$) in Fig. 14.8.

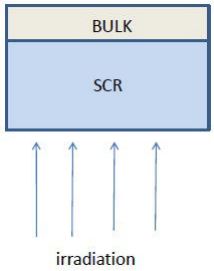

Figure 14.7: Scheme - thin bulk and thick SCR, illumination comes from the side of the SCR

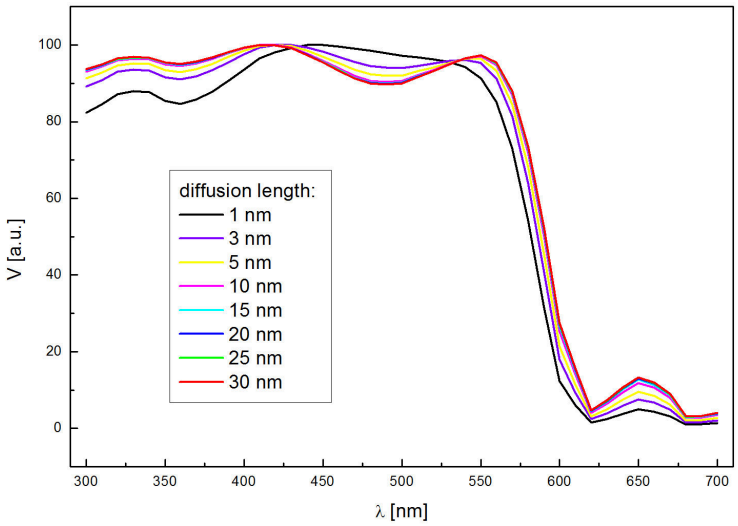

Figure 14.8: Photovoltage spectra - $w = 130nm$, $d = 20nm$ and light comes from the side of the SCR, $L \in < 1; 30 > nm$

Lastly, we assume that the bulk is thick ($d = 130nm$), the space charge region is thin ($w = 20nm$) and irradiation comes from the side of the bulk (Fig.14.10, scheme in Fig.14.9).

In the region with high absorption ($\lambda \sim 480nm$), excitons are generated in the bulk, far away from the bulk/SCR interface. Around the absorption maximum, the measured voltage is strongly dependent on the diffusion length. With increasing diffusion length, the local minimum (around $\lambda = 480nm$) is decreasing (Fig. 14.10). For other wavelengths, excitons are generated closer to the bulk/SCR interface and signal increases.

This situation is particularly suitable for practical estimation of the diffusion length.

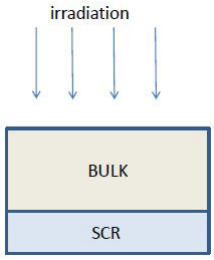

Figure 14.9: Scheme - thick bulk and thin SCR, illumination comes from the side of the bulk

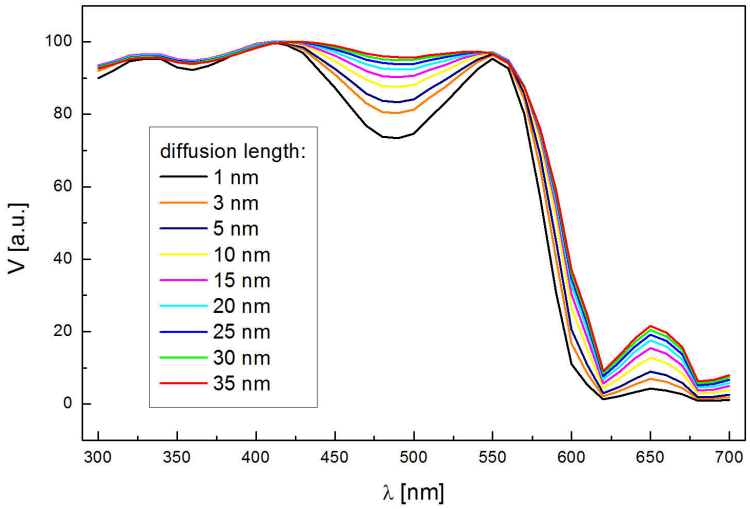

Figure 14.10: Photovoltage spectra - $w = 20nm$, $d = 130nm$ and light comes from the side of the bulk, $L \in < 1; 35 > nm$

In all the calculated spectra (see Fig. 14.4-14.10) one can see interesting phenomenon in the wavelength region $620 - 700nm$. Curves in this region are usually dependent on the diffusion length and they have peaks around wavelength $\lambda = 650nm$. This behaviour is caused by the simplification which was used. We used only one reflectance R (shown in Fig. 14.2) during the calculation of the spectra ($R = R_1 = R_2$) and these peaks are therefore present in our curves. This simplification will not be used during the evaluation of obtained data.

15 SPV measurements on thin polymer layers

15.1 MEH-PPV measurements

We made a number of SPV measurements on thin MEH-PPV layers. Results (and best fits according to Eq. 2.14) of these measurements can be found in Tab. 15.1, graphs are shown in Fig.15.1-15.6. All the samples were illuminated from the side of the bulk.

Thickness of the samples was measured by the ellipsometry measurement. The thickness of samples 1-4 should be just around 80-84 nm. Because of this measurement we try to fit parameters to obtain values similar to the equation $w + d = 80 - 84nm$. In the results of the ellipsometry measurement, there is usually some inaccuracy (around 5%). Therefore the equation $w + d = 80 - 84nm$ is not fully confirmed according to the values shown in Tab. 15.1.

The thickness of samples 5 and 6 was determined (by the ellipsometry measurement) as $w + d = 51nm$.

Parametres in Tab. 15.1 were obtained by fitting the theory to the experimental data of SPV measurements by the method of least squares using Eq.2.14. Spectral dependences of the absorption coefficient α and reflectances R_1 and R_2 were obtained from the optical measurements on MEH-PPV layer. Parameter α is shown in Fig. 14.1 and reflectance $R = R_1$ is in Fig. 14.2. Reflectance R_2 was also measured but in most cases (see Tab. 15.1), R_2 was evaluated as a constant in the whole wavelength region. The only exception was sample 6, where we used measured reflectance R_2 during fitting of the theory to the experimental data. Parameter h_{em} is total thickness of the sample which was obtained from the ellipsometry measurement.

MEH-PPV samples	$L[nm]$	G	$w[nm]$	$d[nm]$	$h_{em}[nm]$	R_2
sample 1	10	0.09	40	30		0.900
sample 2		0.80	65	10	80±4	0.999
sample 3		0.17	77	15	84±4	0.990
sample 4		0.50	60	10		0.999
sample 5	14	0.30	35	15	51±2	0.100
sample 6	14	0.10	30	20	51±2	measured

Table 15.1: Parametres obtained by fitting of the theory to the experimental data (using Eq.2.14) of SPV measurements on thin polymer layers made of MEH-PPV. Total thickness h_{em} of the sample was measured by the ellipsometry measurement.

As we can see in Tab. 15.1, the values of diffusion length are about 10-14 nm and in most cases the space charge region (SCR) is thicker than the bulk. The gain factor G is alternating from 0.09 to 0.80 and it differs for individual samples.

Samples 2, 3 and 4 have similar parameters as the calculated spectra in Fig. 14.6. Their SCR is much thicker than the bulk and the light comes from the side of the bulk. In this situation we are not able to evaluate the diffusion length L. The calculated spectra are almost independent on the diffusion length in the entire wavelength region. Therefore we did not obtain diffusion length L and this parameter is missing in Tab. 15.1.

The compliance of theoretical curves and our experimental measurements is good in the case of samples 1, 5 and 6. The theoretical curve best fits the experimental data from the measurement of sample 6.

The theoretical curves do not fit well in the region of short wavelengths (around $\lambda = 450 - 480nm$). This phenomenon can be seen especially in Fig. 15.2 and Fig. 15.4.

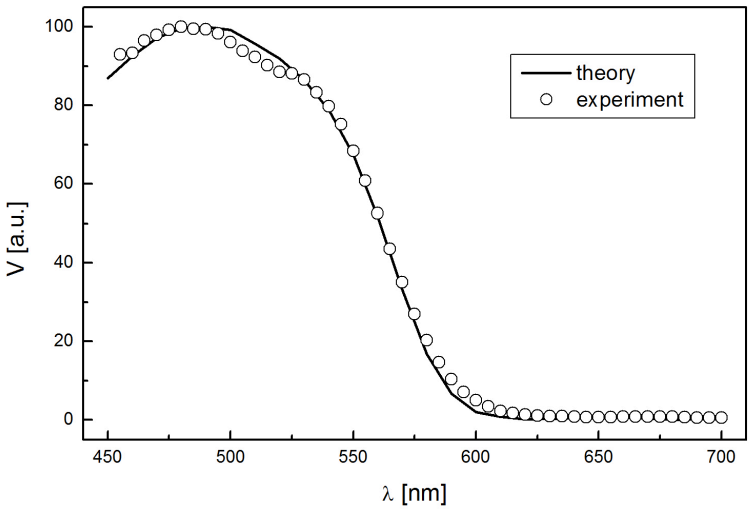

Figure 15.1: Photovoltage spectrum of MEH-PPV - sample 1

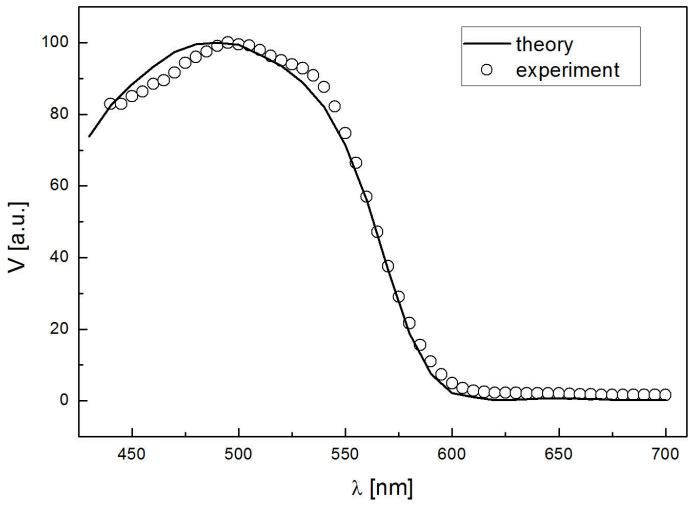

Figure 15.2: Photovoltage spectrum of MEH-PPV - sample 2

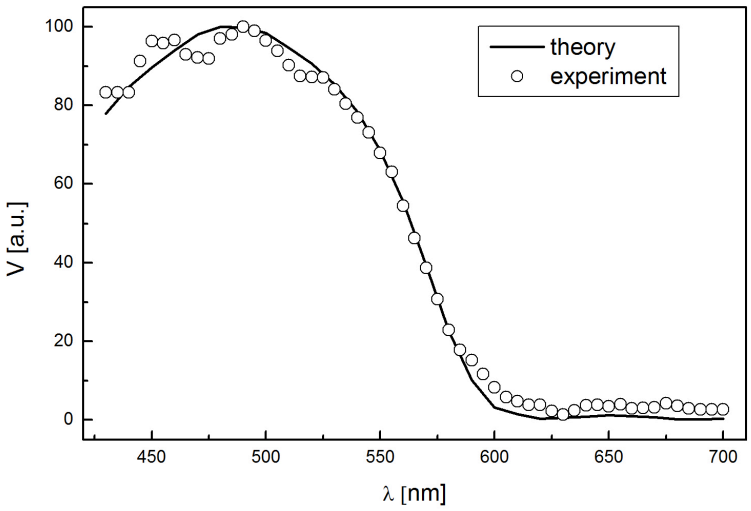

Figure 15.3: Photovoltage spectrum of MEH-PPV - sample 3

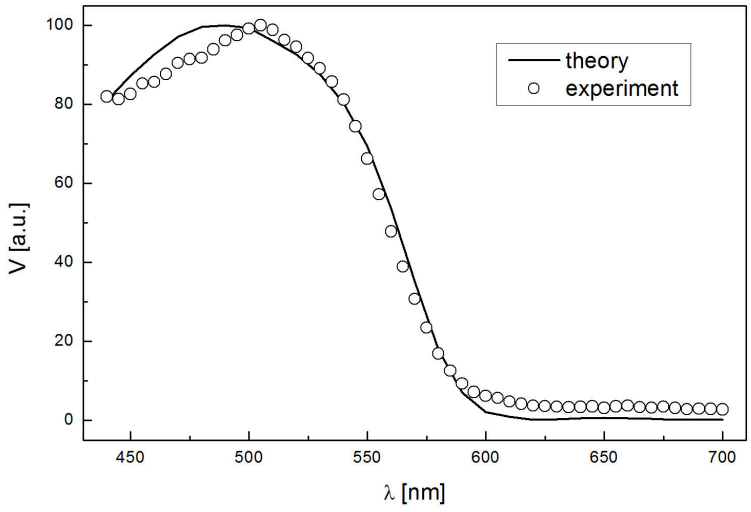

Figure 15.4: Photovoltage spectrum of MEH-PPV - sample 4

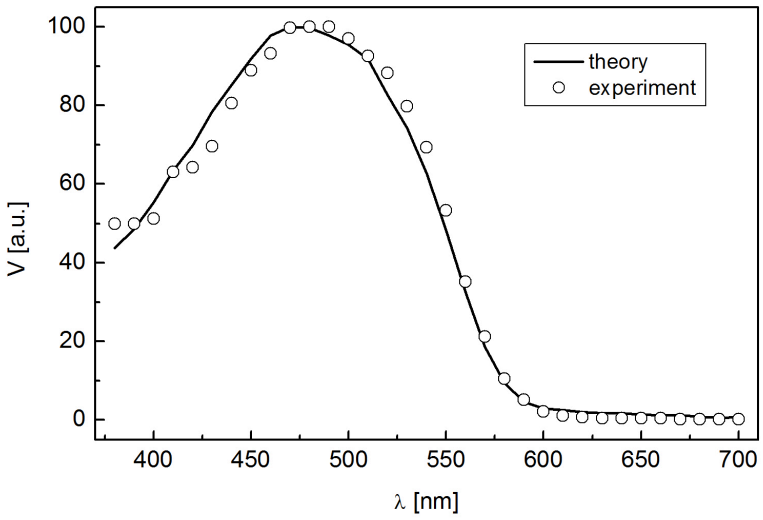

Figure 15.5: Photovoltage spectrum of MEH-PPV - sample 5

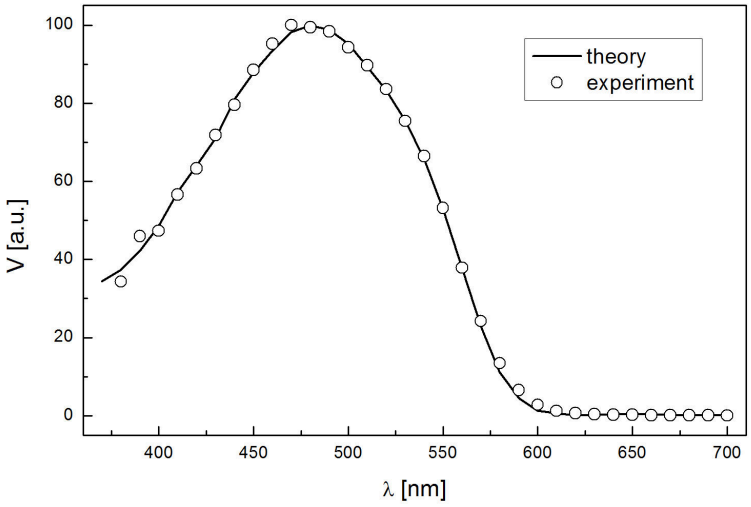

Figure 15.6: Photovoltage spectrum of MEH-PPV - sample 6

15.2 Polythiophene measurements

For the evaluation of the PT photovoltage spectra, the absorption coefficient α and reflectances R_1, R_2 were measured. These parameters are shown in Fig.15.7 (the absorption coefficient α) and the reflectance $R = R_1$ (Fig.15.8). Reflectance R_2 was also measured but this parameter was not used during the evaluation of the spectra. Best fits according to the theory (Eq. 2.14) were obtained for constant values of the parameter R_2. Samples

were illuminated from the side of the bulk and the total thickness of the sample h_{em} was obtained from the ellipsometry measurement.

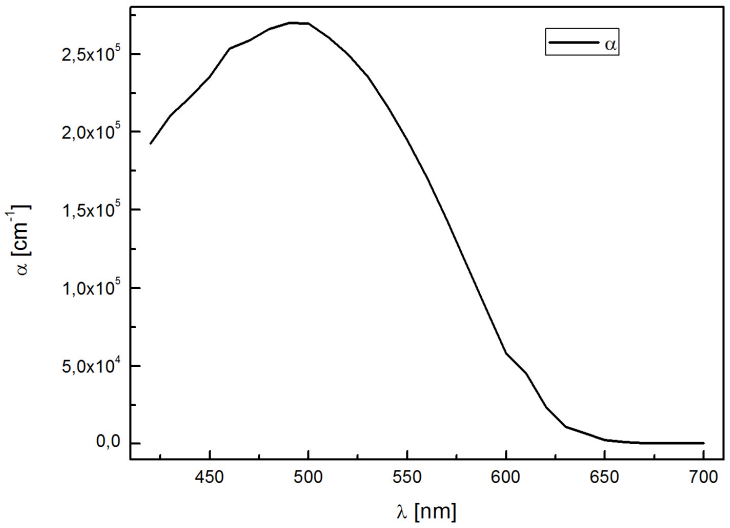

Figure 15.7: Spectrum of the absorption coefficient α of PT

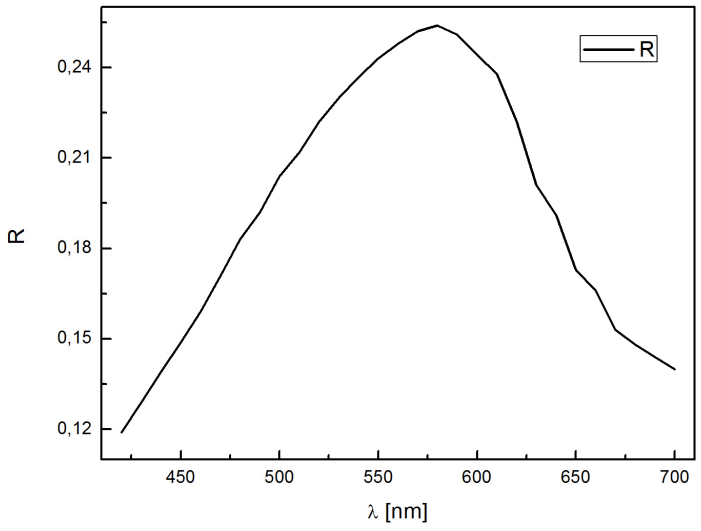

Figure 15.8: Reflectance used for fitting the photovoltage spectra of PT measurements

Comparison of the theoretical curve with the experimental data is in Fig. 15.9 (sample 1) and Fig.15.10 (sample 2).

Results and best fits according to Eq.2.14 from SPV measurements on PT layers can

be found in Tab. 15.2.

PT samples	$L[nm]$	G	$w[nm]$	$d[nm]$	$h_{em}[nm]$	R_2
sample 1	3	0.001	4	100	106±4	0.2
sample 2	9	0.010	5	100	106±4	0.2

Table 15.2: Parametres obtained by fitting of the theory to the experimental data (using Eq.2.14) of SPV measurements on thin polymer layers made of PT. Total thickness h_{em} of the sample was measured by the ellipsometry measurement.

Experimental data of PT photovoltage spectra are appropriate for the evaluation of the diffusion length L. The bulk of the samples is thick, the SCR is thin and the illumination comes from the side of the bulk. This situation is shown in Fig. 14.10 for the calculated spectra and one can see that the calculated curves are dependent on the diffusion length, especially in the wavelength region around the maximum of the absorption coefficient α.

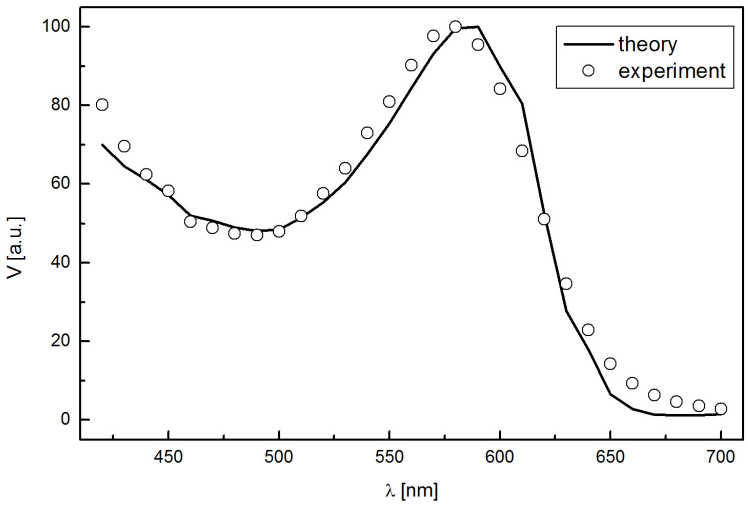

Figure 15.9: Photovoltage spectrum of PT - sample 1

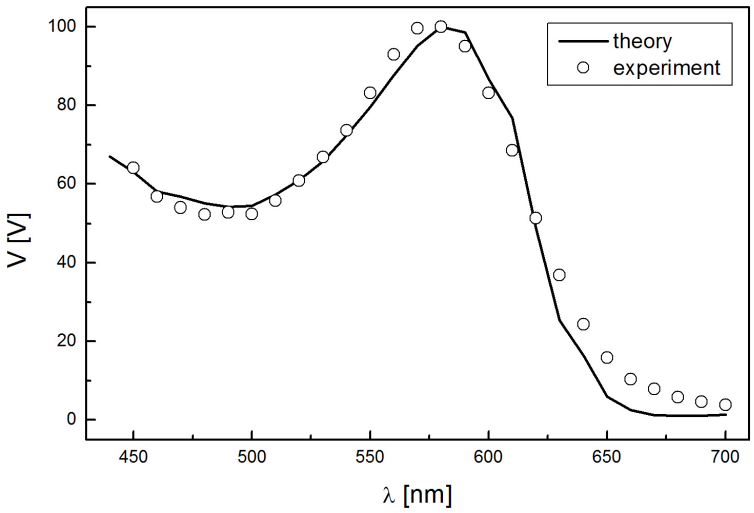

Figure 15.10: Photovoltage spectrum of PT - sample 2

Photovoltage spectra in Fig. 15.9 nad in Fig. 15.10 are quite similar but their diffusion lengths are different (see Tab. 15.2). Comparison of both measured photovoltage PT spectra is shown in Fig. 15.11.

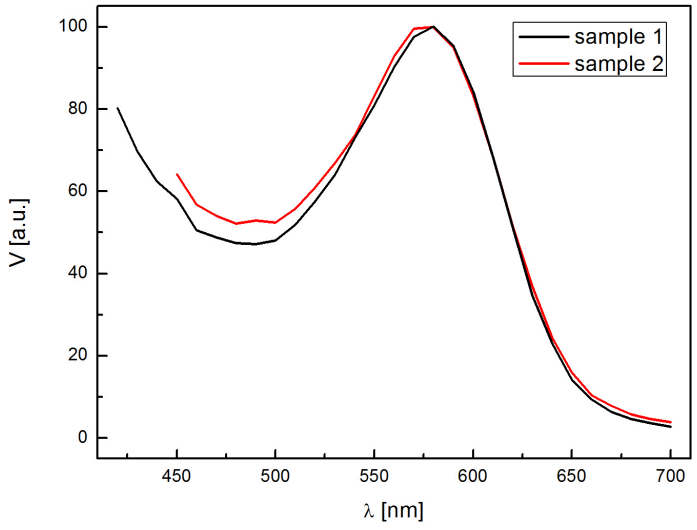

Figure 15.11: Comparison of two measured Polythiophene photovoltage spectra

Fig. 15.11 shows the difference between the spectra. Their parameters are almost the same except the diffusion length L. This variance can be seen in Fig. 15.11 around the maximum of the absorption coefficient ($\lambda \sim 500nm$). Both curves are different around the maximum

and they are dependent on the diffusion length.

15.3 Inaccuracy in obtained parameters

When one looks at Eq. 2.13 and Eq. 2.8, it is obvious that using these equations for fitting of the theory to the experimental photovoltage spectra can be quite difficult. It might appear that the inaccuracy in determination of the parameters (such as diffusion length) is very big and that we can fit the experimental data by almost all values of one parameter by changing other parameters. It is worth to say that it is not true.

On the other hand, not all theoretical curves (see Fig. 15.1-15.6 and Fig. 15.9-15.10) fit the experimental data and the inaccuracy in fitting the experimental data by Eq. 2.14 is not nonzero. We used a specialised programme which was developed for fitting the photovoltage spectra by the method of least squares using Eq. 2.14.

We tried to figure out how big the inaccuracy was. For this experiment, the PT sample 2 was chosen. We changed fitting parametres and we looked at the sum of the least squares method. For some changes of the values of fitting parameters, the sum of the least squares method did not change. By this method, we discovered following inaccuracies for parameters obtained for PT sample 2 : $d \sim 5\%, w \sim 50\%, L \sim 25\%, G \sim 13\%$.

It is worth to say that this method of the evaluation of the inaccuracy can be used only for the experimental data which correspond with theoretical predictions. But it might be a problem in the situations when fitting of the theory to the experimental data shows a higher sum of the least squares method (like spectrum in Fig. 15.1). In this case, the inaccuracy in the evaluation of parameters is higher and it is not possible to state the exact value of obtained parameters.

16 Nanoparticles - Size Determination

16.1 CdS nanoparticles

The image of CdS nanoparticles obtained by TEM is shown in Fig.16.1, together with the histogram which shows particle size distribution. This distribution was obtained by the evaluation of the TEM image.

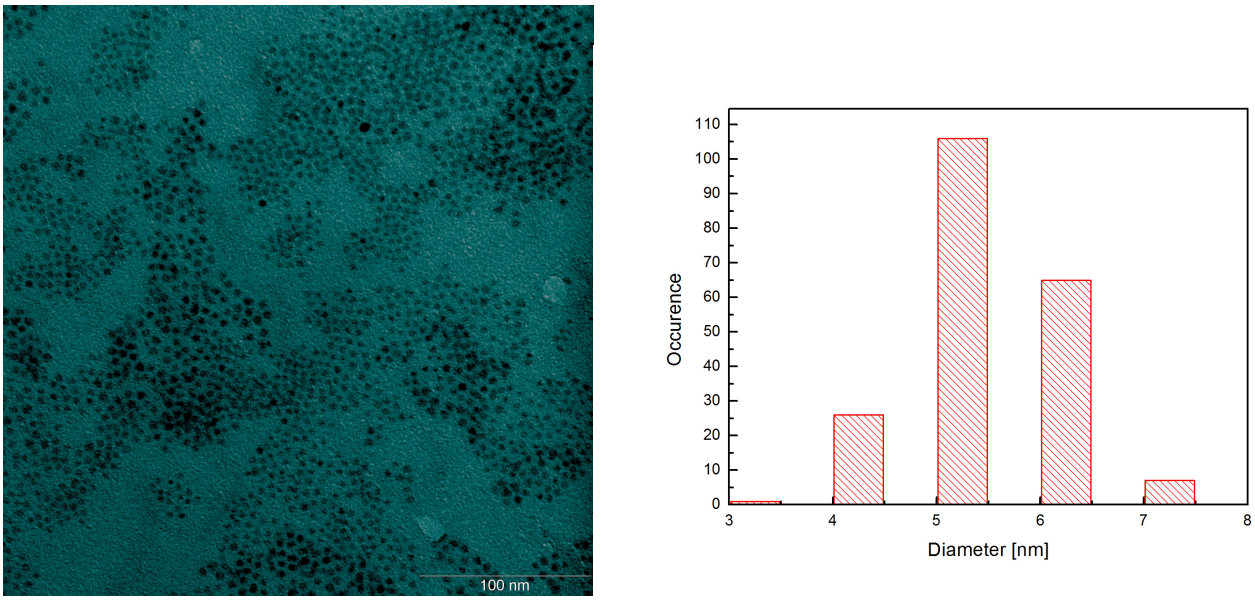

Figure 16.1: TEM image of CdS nanoparticles (left) and histogram showing particle size distribution (right). The histogram was obtained from the evaluation of the TEM image.

Another method for the size determination of nanoparticles was Surface Photovoltage Method (SPV). The experimental data obtained by the SPV measurement can be seen in Fig. 16.2.

Increase of the photovoltage signal starts from the threshold wavelength of $464nm$ (see Fig. 16.2). Using Eq. 3.7 and parameters for CdS nanoparticles ($\epsilon_r = 4.6$, $m_e^* = 0.18m_e$ and $m_h^* = 0.53m_e$ from Ref. [53]), one can obtaine particle diameter $2r = 4.8nm$.

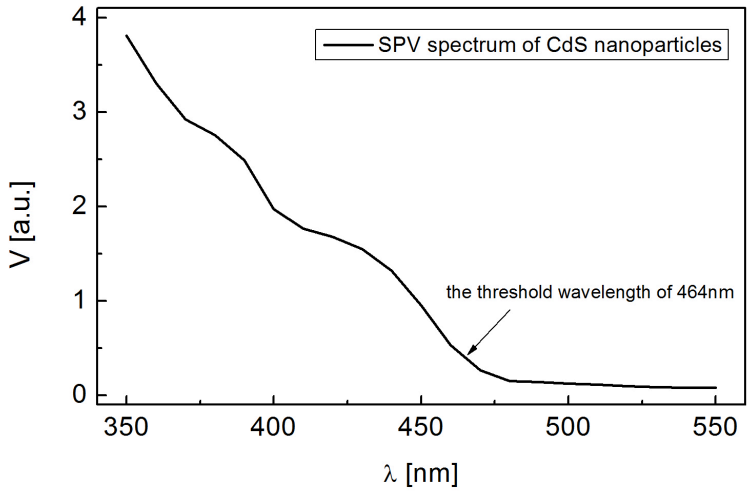

Figure 16.2: Measured photovoltage spectrum of the sample of CdS nanoparticles

For the evaluation of whole obtained photovoltage spectra, we follow approach presented in Ref. [39] for the absorbance spectra. But we use the photovoltage spectra, not the absorbance data.

Assuming that the nanoparticles are spherical and that the absorption coefficient is independent of particle size, we have relation :

$$PV \propto \int_{r}^{\infty} \frac{4}{3}\pi r^3 n(r) dr \tag{16.1}$$

where r is the radius of the nanoparticle and $n(r)$ is the particle size distribution. The particle size distribution can be obtained from measured photovoltage spectra by relation

$$n(r) \propto -\frac{d(PV)/dr}{\frac{4}{3}\pi r^3} \tag{16.2}$$

Radius r was obtained using Eq. 3.7 (with the same parameters as used above) and then the relation 16.2 was used.

Final particle size distribution is shown in Fig. 16.3 together with the histogram from obtained size distribution (which can be easily compared with histogram in Fig. 16.1).

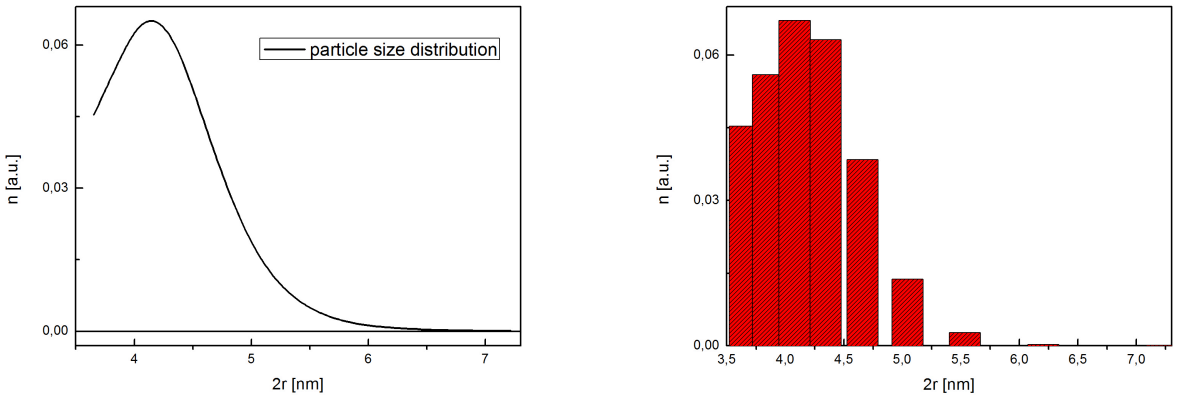

Figure 16.3: Particle size distribution of CdS nanoparticles obtained from measured photovoltage spectrum (left) and this size distribution converted into the histogram (right)

In Tab. 16.1, one can find results of the particle size determination by different methods. The Sigma-Aldrich company states that the size of CdS nanoparticles is about $5nm$. Evaluation of the TEM image showed us particle size from $3nm$ to $7nm$ (see Fig. 16.1) but most CdS particles had diameter $2r \sim 5nm$.

When we used threshold wavelength of the photovoltage spectra (Fig. 16.2), the obtained particle diameter was $2r = (4.8 \pm 0.1)nm$.

Using photovoltage spectra and relation (16.2), we got particle size distribution (see Fig. 16.3) where particle diameter was in range $2r = 3.5nm - 6.5nm$ and most particles had diameters $2r = 4.0 - 4.5nm$.

estimation method	diameter $(=2r)[nm]$
TEM image	$3.0 - 7.0$
treshold wavelength	4.8 ± 0.1
particle size distribution	$3.5 - 6.5$
Sigma Aldrich information	5

Table 16.1: Evaluation of the size distribution of the sample with CdS nanoparticles by different methods.

Transmittance spectra of ITO substrate and ITO substrate covered by CdS nanoparticles were measured by the UV-Vis Absorption Spectroscopy (see Fig. 16.4). Decline of the ITO/CdS transmittance spectrum starts at $\lambda \sim 460nm$ and it continues till $\lambda \sim 350nm$ where glass starts to absorb the light. Transmittance is decreasing in the region of the wavelengths where the photovoltage signal is increasing (see Fig. 16.2).

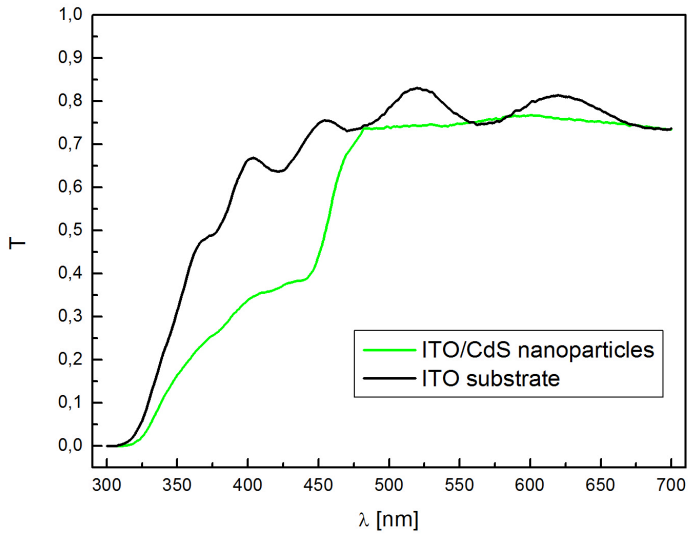

Figure 16.4: Transmittance of ITO substrate and ITO/CdS nanoparticles sample obtained from the UV-Vis Absorption Spectroscopy

The evaluation of CdS nanoparticle size distribution is partly described in Ref.[18] .

16.2 ZnO nanoparticles

Two types of ZnO nanoparticles with different size distribution were used. For type I, the Sigma-Aldrich company states that particle size is $< 50nm$. Type II has particle size $< 130nm$.

16.2.1 Type I

The transmission electron microscopy (TEM) was used for taking images (by a transmission electron microscope Jeol 2000 FX) of ZnO sample. Result of this TEM measurement is in Fig. 16.5. Histogram showing the particle size distribution of ZnO sample is in Fig. 16.5 too.

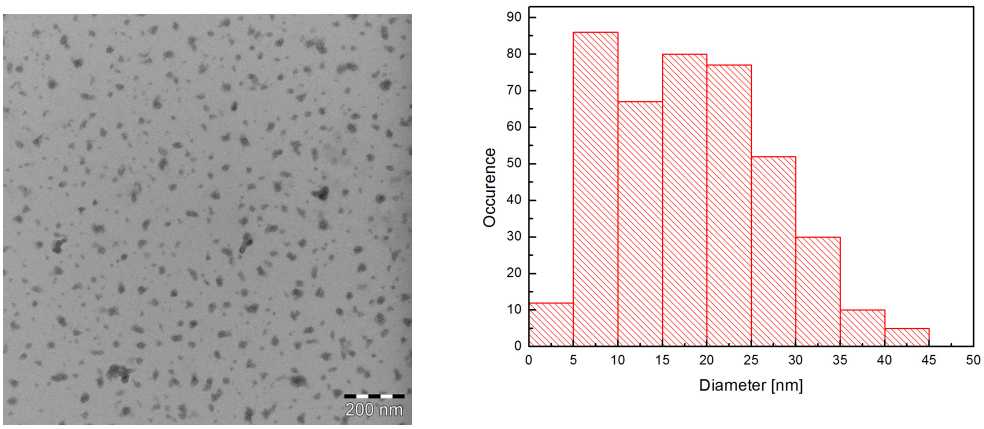

Figure 16.5: TEM image of ZnO nanoparticles-type I (left) and histogram showing particle size distribution (right). The histogram was obtained from the evaluation of the TEM image.

The measured photovoltage spectrum of ZnO nanoparticles type I is shown in Fig. 16.6.

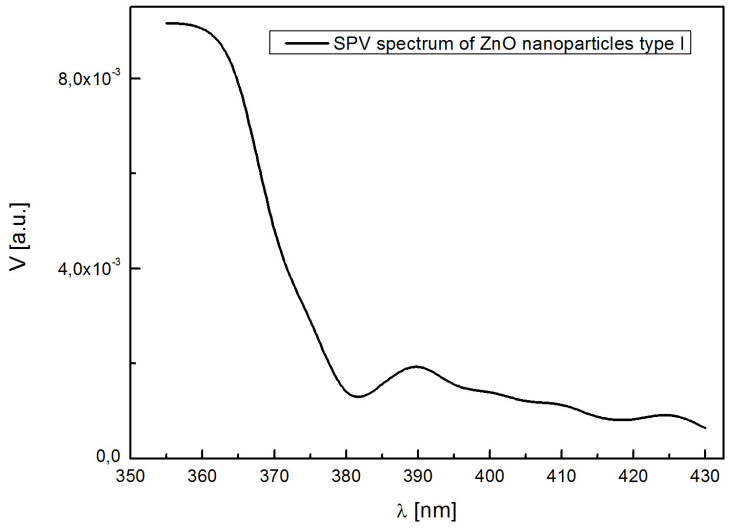

Figure 16.6: Photovoltage spectrum of ZnO nanoparticles (particle size distribution $< 50nm$)

In Fig. 16.6 we can see that the increase of the photovoltage spectrum starts at $380nm$

and maximum is around $360nm$. This behaviour indicates that type I does not have one particle size but particle size distribution is broader. The smallest diameter in the particle size distribution should correspond to the highest value in the photovoltage spectra. For given spectra (Fig. 16.6), this value is for wavelength $\lambda = 360nm$. Using parametres (taken from Ref. [7])$\epsilon_r = 3.7$, $m_e^* = 0.24m_e$ and $m_h^* = 0.45m_e$ and assuming that band gap of bulk ZnO is $3.3eV$, one can get from Eq. 3.7 that smallest particle size is $2r = 4.7nm$.

16.2.2 Type II

Analysis of ZnO nanoparticles type II had started with SEM measurement. Image from this measurement is shown in Fig. 16.7.

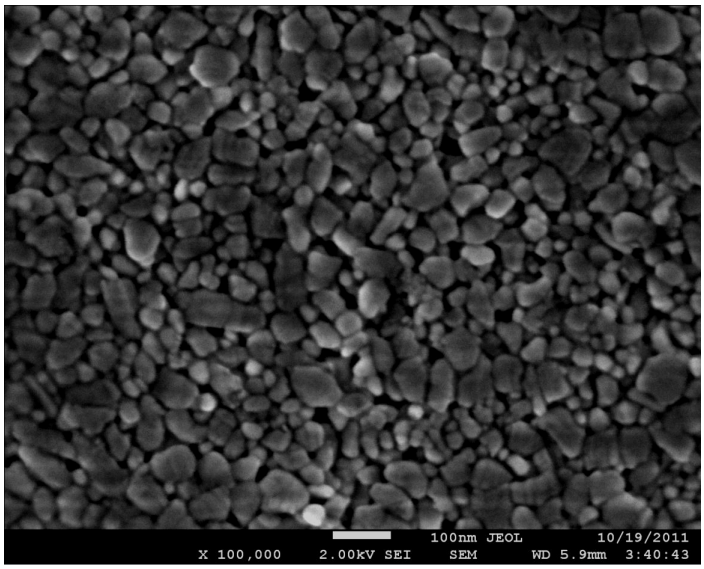

Figure 16.7: SEM image of ZnO nanoparticles-type II

This picture shows us that ZnO nanoparticles type II have broad particle size distribution and we can see the particles in diameter range (approximately) $2r = 10 - 100nm$.
After SEM measurement, the photovoltage spectra were measured. Photovoltage spectra of two different samples with ZnO nanoparticles of type II are shown in Fig. 16.8. We can see that increase of the photovoltage starts around wavelength $385nm$ and maximum is for $335nm$. This indicates that type II has broader distribution of particle size. The smallest particle size should be (for $\lambda = 335nm$, using parametres $\epsilon_r = 3.7$, $m_e^* = 0.24m$, $m_h^* = 0.45m_e$ and band gap of bulk ZnO as $3.3eV$) (by Eq. 3.7) $2r = 3.5nm$.

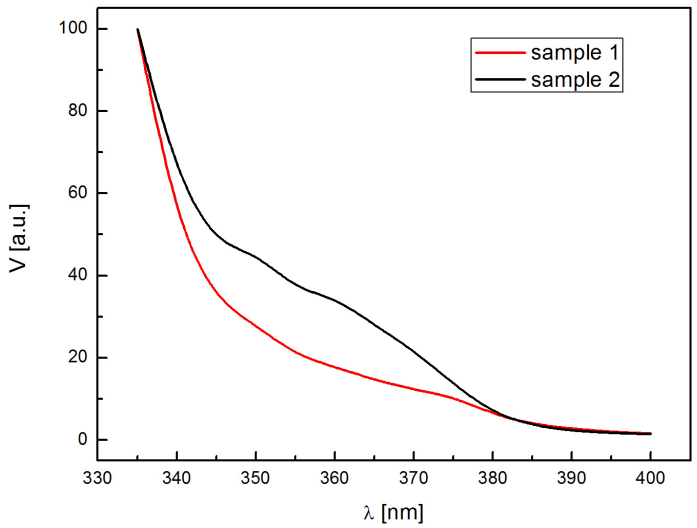

Figure 16.8: Two photovoltage spectra of samples with ZnO nanoparticles-type II (particle size $< 130nm$)

Results of the evaluation of obtained photovoltage spectra show us that small nanoparticles should be present in the particle size distribution. Because of the distinction of the SEM image which is able to show particles with diameter bigger than $\sim 10nm$, we decided to verify the results obtained from the photovoltage spectra. Therefore a TEM measurement was done. Results of this measurement (TEM image and obtained histogram) are shown in Fig. 16.9.

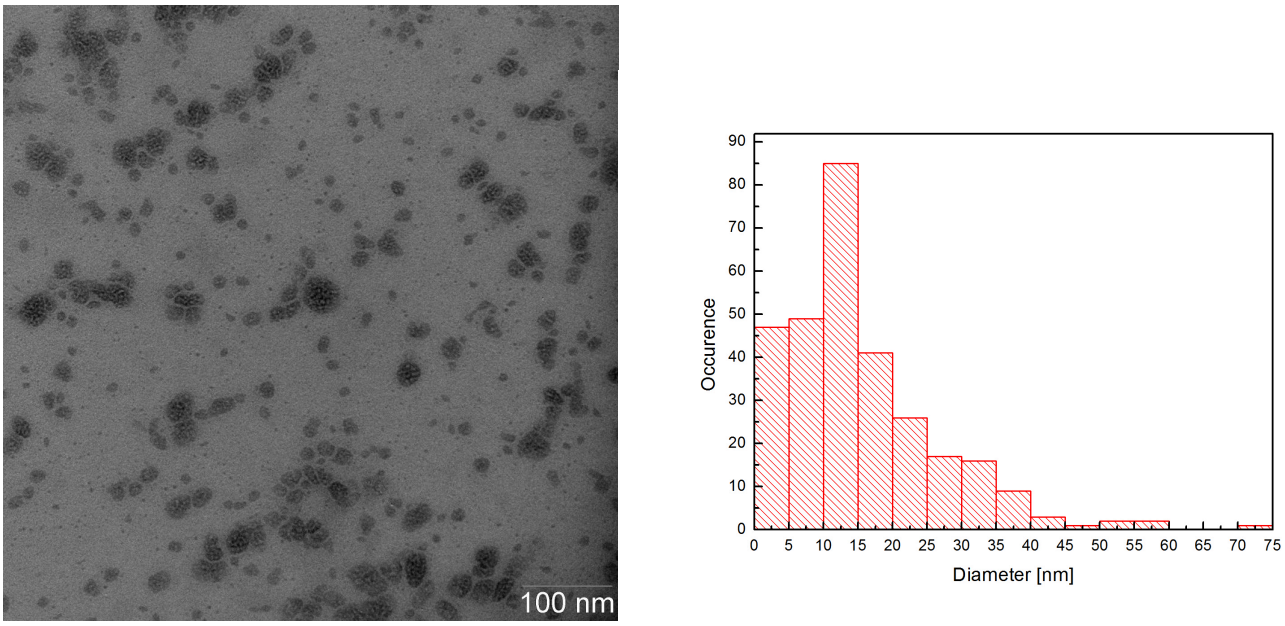

Figure 16.9: TEM image of ZnO nanoparticles type II (left) and histogram showing particle size distribution (right). The histogram was obtained from the evaluation of the TEM image.

Evaluation of the TEM measurement shows broad particle size distribution which also includes small nanoparticles. This final result agrees well with the evaluation of photovoltage spectra (because it shows smaller particles) and it also corresponds with SEM measurement and Sigma-Aldrich information because of the presence of bigger particles in the histogram.

Using UV-Vis Absorption Spectroscopy, the transmittance of both types of ZnO nanoparticles was measured (see Fig. 16.10). One can see that the transmittance spectra are different for individual types of ZnO nanoparticles. This difference is connected to different particle size distribution (see Fig. 16.5 and Fig. 16.9). ZnO nanoparticles with broader particle size distribution and containing bigger particles (type II) have sharper decline of the spectra and this decrease starts at longer wavelengths comparing with type I.

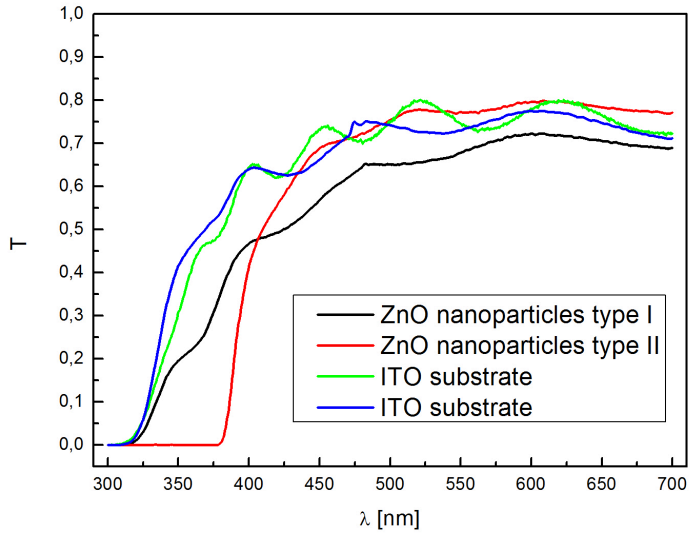

Figure 16.10: UV-Vis Absorption spectra of transmittance of Zno nanoparticles type I and type II and two used ITO substrates

In conclusion, photovoltage spectra of both types of ZnO nanoparticles (type I and type II) show broad particle size distribution (because of gradual increase in Fig. 16.6 and in Fig. 16.8). These broad distributions agree with TEM images and obtained histograms (Fig. 16.5 and Fig. 16.9) and also with SEM image of ZnO nanoaprticles type II (Fig. 16.7).

17 SPV and UV-Vis Absorption Spectroscopy measurements on polymer layers containing inorganic nanoparticles

17.1 Polymer layers containing CdS nanoparticles

MEH-PPV sample with CdS nanoparticles was measured by the SPV method and illumination came from both side (from the SCR and from the bulk). Results of both measurements are shown in Fig. 17.1.

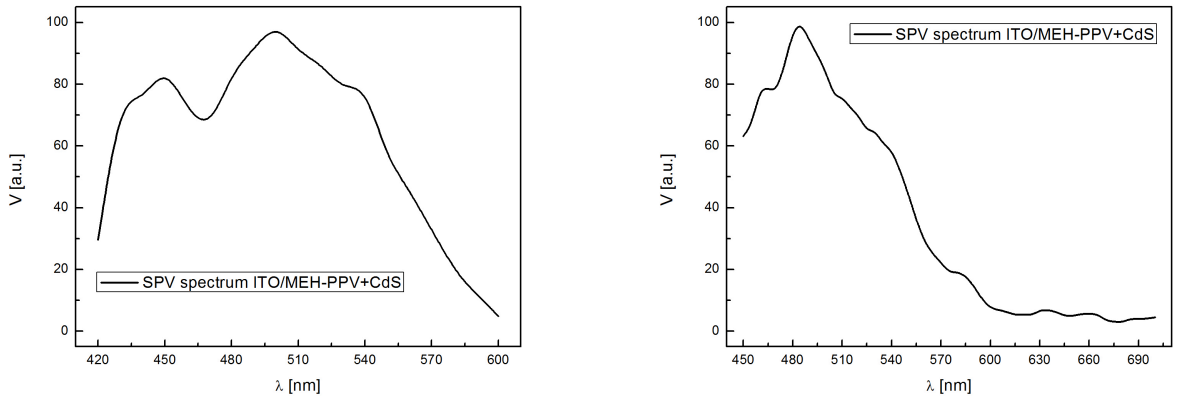

Figure 17.1: Measured photovoltage spectra of ITO/MEH-PPV+CdS sample. Light came from the side of the bulk (left) and from the side of the SCR (right)

One would expect that CdS nanoparticles change photovoltage spectra of the sample. According to the results in Fig. 17.1, it seems that the obtained spectra are similar to photovoltage spectra of MEH-PPV layers without nanoparticles (for instance, see Fig. 15.5). Small peak is situated at $\lambda \sim 450nm$ (for spectrum illuminated from the side of the bulk) and this peak can be connected with presence of CdS nanoparticles in the measured layer. But for the spectrum illuminated from the side of the SCR, maximum is for $\lambda \sim 500nm$ and the peak corresponding to CdS nanoparticles in the layer did not reveal.

Because of little evidence of the influence of CdS nanoparticles in the photovoltage spectra, transmittance spectra were measured using UV-Vis Absorption Spectroscopy (Fig. 17.2).

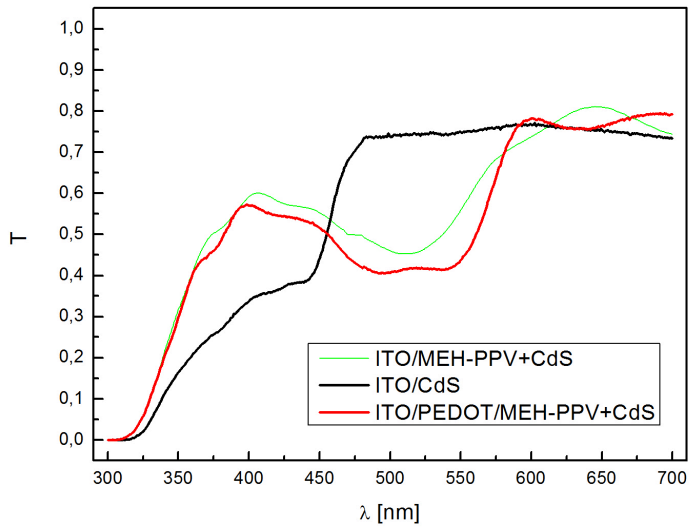

Figure 17.2: Transmittance spectra of samples containing CdS nanoparticles

Spectra of ITO/PEDOT/MEH-PPV+CdS and ITO/MEH-PPV+CdS samples are very similar. Around the maximum of the absorption coefficient of MEH-PPV (see Fig. 14.1), transmittance spectra have local minimum (in range $\lambda = 480 - 550nm$). Transmittance of the ITO substrate covered with CdS nanoparticles has different spectrum - it starts to decrease at $\lambda \sim 480nm$ and spectrum continues to decrease till the range of shorter wavelengths where glass absorbs all illumination.

On the other hand, samples containing both polymer MEH-PPV and CdS nanoparticles have higher transmittance signal around wavelength $\lambda \sim 400nm$. Sample with PEDOT:PSS layer has a bit lower transmittance because PEDOT:PSS layer is able to absorb the light too.

In conclusion, we measured the SPV and UV-Vis Absorption spectra. In the photovoltage spectra, influence of CdS nanoparticles is not fully evident. Together with the UV-Vis Absorption Spectroscopy results, we can say that the mass fraction of CdS nanoparticles in polymer layer is probably quite small and it does not affect the optical properties.

17.2 Polymer layers containing ZnO nanoparticles

Normalized photovoltage spectra of two MEH-PPV samples containing ZnO nanoparticles ("dispersive" and "porous") together with the spectrum of MEH-PPV layer without nanoparticles are shown in Fig. 17.3.

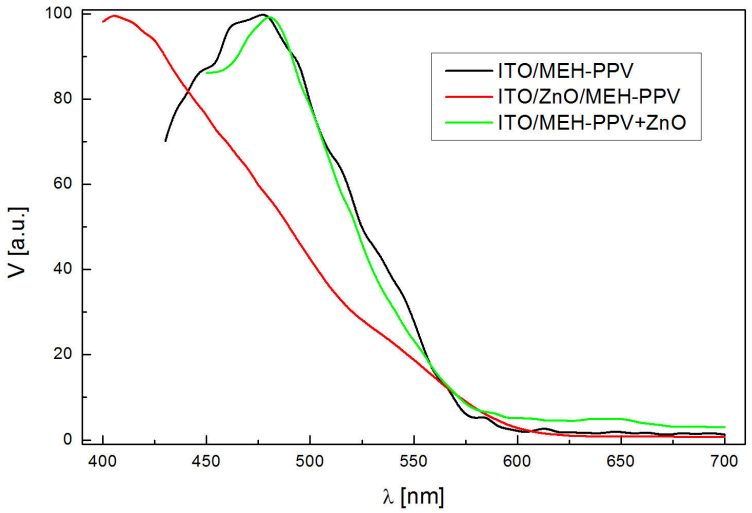

Figure 17.3: Normalized photovoltage spectra of MEH-PPV layer and MEH-PPV layers containing ZnO nanoparticles (illuminated from the side of the SCR)

According to Fig. 17.3, it looks that shapes of the spectra are the same for ITO/MEH-PPV layer and for ITO/MEH-PPV+ZnO layer. "Porous" layer ITO/ZnO/MEH-PPV has different increase and its maximum is situated at shorter wavelength.

This evaluation will rather change when we do not use normalized spectra (see Fig. 17.4). Maximum of "porous" ZnO layer is really at shorter wavelength and its signal is much more stronger than signal of the others. Shape of the spectra measured on ITO/MEH-PPV+ZnO and ITO/MEH-PPV samples are similar but not exactly the same. It seems that the dispersive ZnO sample has similar behaviour as ITO/MEH-PPV sample.

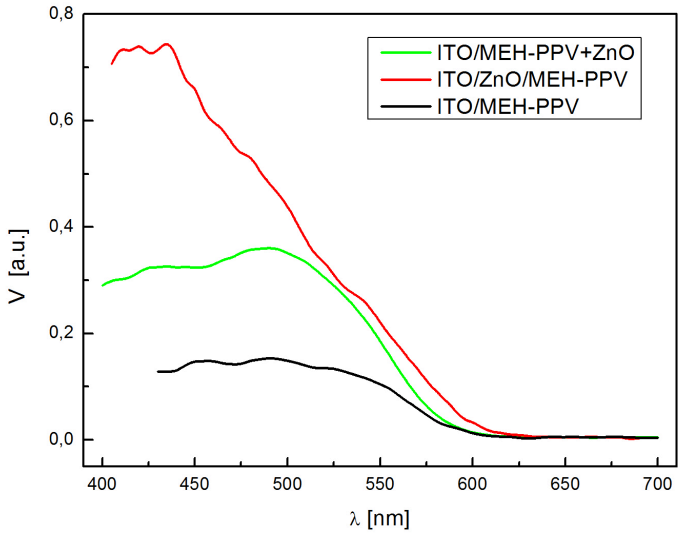

Figure 17.4: Measured photovoltage spectra (illuminated from the side of the bulk) of MEH-PPV layer and MEH-PPV layers containing ZnO nanoparticles

Another interesting question is how the measured spectra look at around $\lambda \sim 400nm$ where ZnO nanoparticles should influence the spectra (according to Fig. 16.6 and Fig. 16.8). The SPV spectra in this region are shown in Fig. 17.5. This figure shows a strong increase of the signal from ITO/ZnO/MEH-PPV sample comparing to ITO/MEH-PPV+ZnO layer. This indicates that the porous ZnO sample is much more influenced by containing ZnO nanoparticles comparing to the dispersive ZnO sample.

This result can be explained by the morphology of the samples. Photovoltage is generated by the dissociation of excitons at the polymer/inorganic nanoparticles interface and then by the transport of the charges to the electrodes. As we can see in Fig. 8.1, the pathways for charges are different because of different preparation techniques. In the dispersive sample, inorganic nanoparticles are dispersed in the polymer and it is very difficult to find percolation path for charges after exciton dissociation (especially if the mass fraction of nanoparticles to polymer is low). But in the porous sample, percolation paths should be present in the sample and charges are able to reach the electrodes. A strong photovoltage signal can therefore be measured in the case of the porous sample.

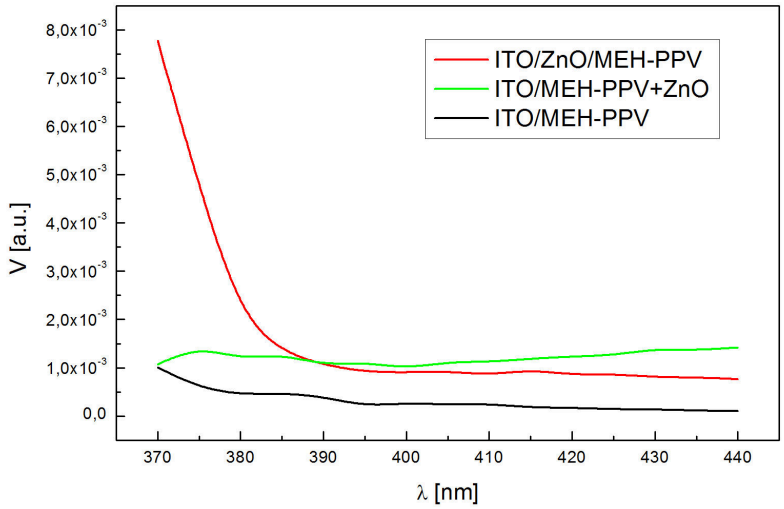

Figure 17.5: Measured photovoltage spectra of MEH-PPV layer and MEH-PPV layers containing ZnO nanoparticles (illuminated from the side of the SCR) showing signal starting to increase around $\lambda = 385nm$

Transmittance spectra were measured on investigated samples (see Fig. 17.6). Results show that transmittance of ITO/MEH-PPV is really similar to transmittance of ITO/MEH-PPV+ZnO. Curve of ITO/ZnO/MEH-PPV is different mainly in short wavelength region. Lowered transmittance in the region of shorter wavelengths corresponds with measured photovoltage spectra.

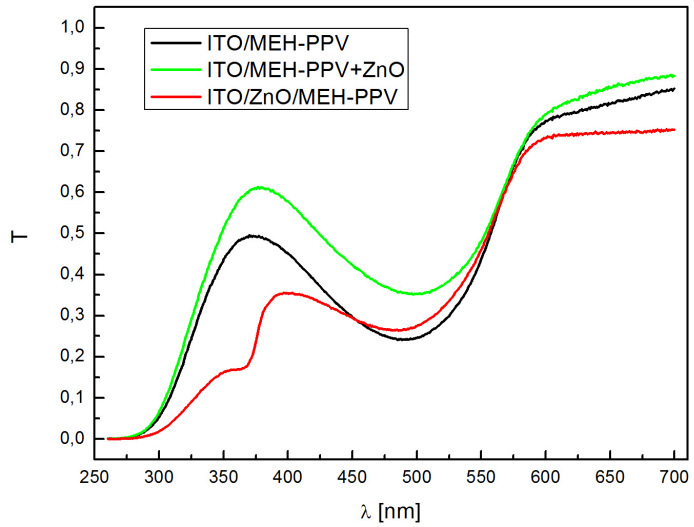

Figure 17.6: Transmittance spectra of samples containing ZnO nanoparticles together with MEH-PPV layer

In conclusion, two different types of MEH-PPV:ZnO samples (with different morphology) were compared with simple MEH-PPV layer. Porous ZnO layer (ITO/ZnO/MEH-PPV) is strongly influenced by the presence of ZnO nanoparticles but dispersive layer (ITO/MEH-PPV+ZnO) has similar properties as MEH-PPV layer. This behaviour is probably caused by low mass fraction of ZnO nanoparticles in MEH-PPV layer (dispersive sample).

Part V

Conclusion

We used few different experimental techniques for the evaluation of polymer and inorganic materials. To characterize the polymer layers dark current-voltage and photovoltage spectra were measured.

Several interesting parameters were obtained from the measurements of dark J-V characteristics at different temperatures. We used "hole-only" regime and we evaluated the density of traps for MEH-PPV layers as $H_b = 5,7.10^{17} cm^{-3}$ or $H_b = 3,8.10^{18} cm^{-3}$ respectively. The mobility of the free holes at room temperature was determined from the Ohmic region of MEH-PPV layer as $\mu = 3,4.10^{-6} cm^2 V^{-1} s^{-1}$ and $\mu = 8,2.10^{-7} cm^2 V^{-1} s^{-1}$ respectively. For the Polythiophene layer, the mobility of the free holes obtained from the Ohmic region was $\mu = 4,7.10^{-5} cm^2 V^{-1} s^{-1}$. The compliance of our results with parameters which can be found in the literature is very good. We believe that all the measured dark J-V characteristics are controlled by the SCLC model with the exponential distribution of the traps.

The Surface Photovoltage Method was discussed and we showed some calculations which can show different properties of measured photovoltage spectra. Experimental data were obtained from SPV measurements on MEH-PPV and PT samples. All the measured spectra were evaluated and we determined (if it was possible) important parameters, such as exciton diffusion length L. For the MEH-PPV layers, we got diffusion length as $L = 10 - 14nm$. Measured PT layers had diffusion length shorter, obtained values are $L = 3 - 9nm$.

An interesting goal in the field of the polymer photovoltaics is preparation of an efficient hybrid inorganic-organic solar cell. For this purpose, we evaluated polymer layers containing inorganic nanoparticles.

We evaluated particle size distribution of CdS and two types of ZnO nanoparticles. Few different experimental techniques were used for this task - TEM (SEM) measurements, measurements of the photovoltage spectra and we also used UV-Vis Absorption Spectroscopy. We obtained almost the same particle size distributions of CdS nanoparticles by TEM measurements and by evaluation of the photovoltage spectra. As regards two different types of ZnO nanoparticles, we were able to get smallest particle diameter in the distribution from the photovoltage spectra and this diameter is the same as from the TEM measurements. The compliance of obtained particle size distributions with the information of the company which sells the inorganic particles is very good.

CdS nanoparticles were mixed with the MEH-PPV solution and resulting layers were measured by the SPV method and by the UV-Vis Absorption Spectroscopy too. Measured spectra were similar to the spectra obtained from MEH-PPV layers (without nanoparticles). This is probably caused by the low mass fraction of CdS nanoparticles to polymer material.

Hybrid polymer-ZnO nanoparticles layers were prepared by two different methods. First

method consists of mixing MEH-PPV solution with ZnO nanoparticles (similar to preparation of MEH-PPV/CdS layers). Second method was different - onto ITO substrate ZnO solution was firstly spincoated and then MEH-PPV layer was added. This second method should be more useful for preparing hybrid layers. This prediction was confirmed - the measured spectra (both by the SPV method and by the UV-Vis Absorption Spectroscopy) in the first case did not reflect the presence of the nanoparticles as one can expect. The measured spectra are similar (but not exactly the same) as spectra of MEH-PPV layers without nanoparticles. This could be connected with the low mass fraction of ZnO nanoparticles to MEH-PPV material. Layers made by the second method were different. It is possible that percolation pathways for charges after exciton dissociation at the polymer/ZnO interface were made and measured spectra (clearly showing presence of ZnO nanoparticles) are obviously different from spectra of MEH-PPV layers and also from spectra of MEH-PPV+ZnO layers made by the first method.

Future research in the field of organic semiconducting polymers (related to the presented diploma thesis) can focus on the improvement of stability of various polymer layers. For instance measuring of dark J-V characteristics on polymer layers with various thickness at different temperatures would be a very interesting method for the evaluation of important parameters.

As regards hybrid organic/inorganic layers, very promising is the preparation of "porous" samples where inorganic nanoparticles are spincoated onto the substrate and then the polymer layer is spincoated onto the inorganic layer. The polymer layer tends to penetrate through the nanoparticles and a large organic/inorganic interface appears. The main goal of this research is fabrication of very efficient hybrid organic solar cell but further investigation is needed in this field.

Bibliography

[1] S. D. Baranovskii, H. Cordes, F. Hensel, and G. Leising. Charge-carrier transport in disordered organic solids. *Physical Review B*, 62(12):7934–7938, 2000. PRB.

[2] S.D. Baranovskii, I.P. Zvyagin, H. Cordes, S. Yamasaki, and P. Thomas. Electronic transport in disordered organic and inorganic semiconductors. *Journal of non-crystalline solids*, 299:416–419, 2002.

[3] Baptiste Billaud and T.T. Truong. Quantum properties of spherical semiconductor quantum dots. *arXiv preprint arXiv:1107.4159*, 2012.

[4] A.R. Blythe and D. Bloor. *Electrical Properties of Polymers*. Cambridge University Press, New York, 2005.

[5] Christoph Brabec, Ullrich Scherf, and Vladimir Dyakonov. *Organic photovoltaics: materials, device physics, and manufacturing technologies*. Wiley-vch, 2011.

[6] Christopher M. A. Brett and Ana Maria Oliviera Brett. *Electrochemistry Principles, Methods, and Applications*. Oxford University Press, New York, 1993.

[7] Louis E. Brus. Electron/electron and electron/hole interactions in small semiconductor crystallites: The size dependence of the lowest excited electronic state. *The Journal of chemical physics*, 80:4403, 1984.

[8] Wolfgang Brutting. *Physics of Organic Semiconductors*. WILEY-VCH, Weinheim, 2005.

[9] Xin Chen. *Synthesis and Characterization of Polythiophene Derivatives*. PhD thesis, 2007.

[10] Z. Chiguvare, J. Parisi, and V. Dyakonov. Current limiting mechanisms in indium tin oxide/poly3 hexylthiophene/aluminum thin film devices. *Journal of Applied Physics*, 94(4):2440–2448, 2003.

[11] Veaceslav Coropceanu, Jerome Cornil, Demetrio A. da Silva Filho, Yoann Olivier, Robert Silbey, and Jean-Luc Bredas. Charge transport in organic semiconductors. *Chemical Reviews-Columbus*, 107(4):926–952, 2007.

[12] Alvin M. Goodman. A method for the measurement of short minority carrier diffusion lengths in semiconductors. *Journal of Applied Physics*, 32(12):2550–2552, 1961.

[13] Serap Gunes, Helmut Neugebauer, and Niyazi Serdar Sariciftci. Conjugated polymer-based organic solar cells. *Chemical Reviews-Columbus*, 107(4):1324–1338, 2007.

[14] Jonathan J.M. Halls and Richard H. Friend. Organic photovoltaic devices. *Clean Electricity from Photovoltaics*, page 377, 2001.

[15] Behrang Homayoun Hamadani. *Electronic charge injection and transport in organic field-effect transistors*. PhD thesis, 2007.

[16] N. M. Huang, C. S. Kan, P. S. Khiew, and S. Radiman. Single w/o microemulsion templating of cds nanoparticles. *Journal of Materials Science*, 39(7):2411–2415, 2004.

[17] G.R. Hutchison, Yu-Jun Zhao, B. Delley, A.J. Freeman, M.A. Ratner, and T.J. Marks. Electronic structure of conducting polymers: Limitations of oligomer extrapolation approximations and effects of heteroatoms. *Physical Review B*, 68(3):035204, 2003.

[18] Touskova J., Tousek J., Remes Z., Polonskyi O., Kousal J., Rohovec J., Kuritka I., and Schauer F. Exciton diffusion length in meh-ppv and cds nanoparticles size distribution by surface photovoltage method. In *26th European Photovoltaic Solar Energy Conference and Exhibition*. WIP Munchen Germany.

[19] S.C. Jain, Wim Geens, Anupama Mehra, Vikram Kumar, Tom Aernouts, Jef Poortmans, Robert Mertens, and M. Willander. Injection-and space charge limited-currents in doped conducting organic materials. *Journal of Applied Physics*, 89(7):3804–3810, 2001.

[20] S.C. Jain, Ashok Kapoor, Wim Geens, Jef Poortmans, Robert Mertens, and Magnus Willander. Trap filled limit of conducting organic materials. *Journal of Applied Physics*, 92(7):3752–3754, 2002.

[21] Suresh C. Jain, M. Willander, and V. Kumar. *Conducting Organic Materials and Devices*, volume 81 of *Semiconductors and Semimetals*. Elsevier Inc., 2007.

[22] Anderson Janotti and Chris G. Van de Walle. Fundamentals of zinc oxide as a semiconductor. *Reports on Progress in Physics*, 72(12):126501, 2009.

[23] Ashok K. Kapoor, S.C. Jain, Jef Poortmans, Vikram Kumar, and Robert Mertens. Temperature dependence of carrier transport in conducting polymers: Similarity to amorphous inorganic semiconductors. *Journal of Applied Physics*, 92(7):3835–3838, 2002.

[24] Frederik C. Krebs. Fabrication and processing of polymer solar cells: A review of printing and coating techniques. *Solar Energy Materials and Solar Cells*, 93(4):394–412, 2009.

[25] Pankaj Kumar, S.C. Jain, Aparna Misra, M.N. Kamalasanan, and Vikram Kumar. Characteristics of a conducting organic diode with finite (nonzero) schottky barrier. *Journal of Applied Physics*, 100(11):114506–114506–5, 2006.

[26] Vikram Kumar, S.C. Jain, A.K. Kapoor, Jef Poortmans, and Robert Mertens. Trap density in conducting organic semiconductors determined from temperature dependence of j/v characteristics. *Journal of Applied Physics*, 94(2):1283–1285, 2003.

[27] Vikram Kumar, S.C. Jain, Ashok K. Kapoor, Wim Geens, Tom Aernauts, Jef Poortmans, and Robert Mertens. Carrier transport in conducting polymers with field dependent trap occupancy. *Journal of Applied Physics*, 92(12):7325–7329, 2002.

[28] Wonjoo Lee, Seung-Jae Roh, Kyung-Hee Hyung, Joonyoung Park, Soo-Hyoung Lee, and Sung-Hwan Han. Photoelectrochemically polymerized polythiophene layers on ruthenium photosensitizers in dye-sensitized solar cells and their beneficial effects. *Solar Energy*, 83(5):690–695, 2009.

[29] P.E. Lippens and M. Lannoo. Calculation of the band gap for small cds and zns crystallites. *Physical Review B*, 39(15):10935, 1989.

[30] M.M. Mandoc. *Device physics of all-polymer solar cells.* PhD thesis, 2009.

[31] Sipho Enos Mavundla. *One-dimensional Nanostructured Polymeric Materials for Solar Cell Applications.* PhD thesis, 2010.

[32] Lhadi Merhari. *Hybrid nanocomposites for nanotechnology.* Springer, 2009.

[33] Don Monroe. Hopping in exponential band tails. *Physical Review Letters*, 54(2):146–149, 1985. PRL.

[34] Attila J. Mozer and Niyazi Serdar Sariciftci. Conjugated polymer photovoltaic devices and materials. *Comptes Rendus Chimie*, 9(5/6):568–577, 2006.

[35] K. Norrman, A. Ghanbari-Siahkali, and N. B. Larsen. 6 studies of spin-coated polymer films. *Annual Reports Section "C" (Physical Chemistry)*, 101(0):174–201, 2005.

[36] Jean-Michel Nunzi. Organic photovoltaic materials and devices. *Comptes Rendus Physique*, 3(4):523–542, 2002.

[37] Stefan Daniel Oosterhout. *Hybrid polymer solar cells based on ZnO.* PhD thesis, 2011.

[38] I. D. Parker. Carrier tunneling and device characteristics in polymer light emitting diodes. *Journal of Applied Physics*, 75(3):1656–1666, 1994.

[39] Noshir S. Pesika, Kathleen J. Stebe, and Peter C. Searson. Relationship between absorbance spectra and particle size distributions for quantum-sized nanocrystals. *The Journal of Physical Chemistry B*, 107(38):10412–10415, 2003.

[40] Klaus Petritsch. *Organic Solar Cell Architectures.* PhD thesis, 2000.

[41] R. Rossetti, J.L. Ellison, J.M. Gibson, and L.E. Brus. Size effects in the excited electronic states of small colloidal cds crystallites. *The Journal of chemical physics*, 80:4464, 1984.

[42] Klaus D. Sattler. *Handbook of nanophysics - Nanoparticles and Quantum Dots*. CRC Press, 2011.

[43] J. Campbell Scott. Metal organic interface and charge injection in organic electronic devices. *Journal of Vacuum Science and Technology A Vacuum, Surfaces, and Films*, 21(3):521–531, 2003.

[44] Nobuyuki Sekine, Cheng-Hsuan Chou, Wei Lek Kwan, and Yang Yang. Zno nano-ridge structure and its application in inverted polymer solar cell. *Organic Electronics*, 10(8):1473–1477, 2009.

[45] Franky So. *Organic Electronics: Materials, Processing, Devices and Applications*. CRC Press, 2010.

[46] J. Tousek and J. Touskova. A novel approach to the surface photovoltage method. *Solar Energy Materials and Solar Cells*, 92(9):1020–1024, 2008.

[47] J. Tousek, J. Touskova, Z. Remes, J. Cermak, J. Kousal, D. Kindl, and I. Kuritka. Exciton diffusion length and concentration of holes in meh-ppv polymer using the surface voltage and surface photovoltage methods. *Chemical Physics Letters*, 552:49–52, 2012.

[48] J. Tousek, J. Touskova, Z. Remes, J. Kousal, S. A. Gevorgyan, and F. C. Krebs. Exciton diffusion length in some thermocleavable polythiophenes by the surface photovoltage method. *Synthetic Metals*, 161(23/24):2727–2731, 2012.

[49] Jiri Tousek, Jana Touskova, Ivo Krivka, Petra Pavlackova, Drahomir Vyprachticky, and Vera Cimrova. Surface photovoltage method for evaluation of exciton diffusion length in fluorene-thiophene based copolymers. *Organic Electronics*, 11(1):50–56, 2010.

[50] Deepak Verma, A. Ranga Rao, and V. Dutta. Surfactant-free cdte nanoparticles mixed meh-ppv hybrid solar cell deposited by spin coating technique. *Solar Energy Materials and Solar Cells*, 93(9):1482–1487, 2009.

[51] W.Hu, F.Bai, X.Gong, X.Zhan, H.Fu, and T. Bjornhom. *Organic Optoelectronics*. John Wiley and Sons, 2012.

[52] Raghvendra S. Yadav, Priya Mishra, Rupali Mishra, Manvendra Kumar, and Avinash C. Pandey. Growth mechanism and optical property of cds nanoparticles synthesized using amino-acid histidine as chelating agent under sonochemical process. *Ultrasonics sonochemistry*, 17(1):116–122, 2010.

[53] Shao Min Zhou. Dielectric properties of phase size control cds nanoparticles and conventional powders. *Physica status solidi (a)*, 200(2):423–428, 2003.

List of Tables

List of Symbols and Abbreviations

α - absorption coefficient

β, β_{ef} - slope of the field-dependent mobility

ϵ_0 - permittivity of the vacuum

ϵ_r- relative permittivity

ρ_1- optical reflection coefficient at the illuminated surface

Λ - energetic disorder

Σ- geometric randomness

$\theta_{a,d}$ - ratio of free to trapped carriers (in different energy distributions)

σ - conductivity

ς - Planck constant

$\hbar$ - reduced Planck constant

Δ - intrinsic potential barrier

λ - wavelength

μ - mobility

ω - angular velocity

φ - height of a barrier

ϖ - reduced effective mass

Φ - hopping probability

ϕ_B - Schottky barrier

C - integration constant

d - bulk thickness

D - exciton diffusion coefficient

E_t - energy of the trap depth

F - electric field strength

G - factor of recombination losses in the space charge region

h - thickness of a layer

$H_{a,d}$ - trap density (in different energy distributions)

I - current

I_0- photon flux density

I_p - the ionization potential of the organic material

J - current density

k - electron transport rate

k_B - Boltzmann constant

l_1 - depth of the space charge layer at the illuminated surface

L - diffusion length

m_e - mass of the electron

m_e^* - effective mass of the electron

m_h^* - effective mass of the hole

n - concentration of the carriers

$\Delta n(x)$ - concentration of excess excitons at depth x in the bulk

$n(r)$ - particle size distribution

p - density of free holes

p_t - trapped hole density

q - elementary charge

Q - photon quantum efficiency for hole-electron pair creation

r - radius of the nanoparticles

R - reflectance

s - surface recombination velocity

T - absolute temperature

V - voltage

w - thickness of the space charge region

u, z - empirical constants (for description of the spincoating technique)

W - metal work function

HOMO - Highest Occupied Molecular Orbital

ITO - Indium tin oxide

LUMO - Lowest Unoccupied Molecular Orbital

MEH-PPV - Poly[2-methoxy-5-(2-ethylhexyloxy)-1,4-phenylenevinylene]

PEDOT:PSS - Poly(3,4-ethylenedioxythiophene):Poly(styrenesulfonate)

PT - Polythiophene

SCR - Space Charge Region

SEM - Scanning electron microscopy

SPV - Surface Photovoltage Method

TEM - Transmission electron microscopy

UV-Vis - Ultraviolet–visible spectroscopy